MARTIN MARIETTA ENERGY SYSTEMS LIBRARIES

3 4456 0387078 2

ORNL/TM-12712

ornl

OAK RIDGE NATIONAL LABORATORY

MARTIN MARIETTA

An Examination of the Elastic Structural Response of the Advanced Neutron Source Fuel Plates

OAK RIDGE NATIONAL LABORATORY
CENTRAL RESEARCH LIBRARY
CIRCULATION SECTION
4500N ROOM 175
LIBRARY LOAN COPY
DO NOT TRANSFER TO ANOTHER PERSON
If you wish someone else to see this report, send in name with report and the library will arrange a loan.
DOE-2589 (3-9-77)

Advanced Neutron Source

MANAGED BY
MARTIN MARIETTA ENERGY SYSTEMS, INC.
FOR THE UNITED STATES
DEPARTMENT OF ENERGY

This report has been reproduced directly from the best available copy.

Available to DOE and DOE contractors from the Office of Scientific and Technical Information, P.O. Box 62, Oak Ridge, TN 37831; prices available from (615) 576-8401, FTS 626-8401.

Available to the public from the National Technical Information Service, U.S. Department of Commerce, 5285 Port Royal Rd., Springfield, VA 22161.

This report was prepared as an account of work sponsored by an agency of the United States Government. Neither the United States Government nor any agency thereof, nor any of their employees, makes any warranty, express or implied, or assumes any legal liability or responsibility for the accuracy, completeness, or usefulness of any information, apparatus, product, or process disclosed, or represents that its use would not infringe privately owned rights. Reference herein to any specific commercial product, process, or service by trade name, trademark, manufacturer, or otherwise, does not necessarily constitute or imply its endorsement, recommendation, or favoring by the United States Government or any agency thereof. The views and opinions of authors expressed herein do not necessarily state or reflect those of the United States Government or any agency thereof.

ORNL/TM-12712

Engineering Technology Division

AN EXAMINATION OF THE ELASTIC STRUCTURAL RESPONSE OF THE ADVANCED NEUTRON SOURCE FUEL PLATES

W. F. Swinson
C. R. Luttrell
G. T. Yahr

September 1994

Prepared by the
OAK RIDGE NATIONAL LABORATORY
Oak Ridge, Tennessee 37831
managed by
MARTIN MARIETTA ENERGY SYSTEM, INC.
for the
U.S. DEPARTMENT OF ENERGY
under contract DE-AC05-84OR21400

MARTIN MARIETTA ENERGY SYSTEMS LIBRARIES

3 4456 0387078 2

CONTENTS

Page

LIST OF FIGURES v

ACRONYMS AND SYMBOLS vii

ABSTRACT 1

1. INTRODUCTION 1

2. PLATE RESPONSE TO COOLANT FLOW 3

3. PLATE RESPONSE TO THERMAL EFFECTS 17

4. CONCLUSIONS AND RECOMMENDATIONS 19

5. REFERENCES 21

Appendix A. INVOLUTE BOUNDARY LOADS WITH ENERGY TECHNIQUES A-1

Appendix B. INVOLUTE DEFLECTION USING THE DUMMY-LOAD TECHNIQUE B-1

Appendix C. STRESS CALCULATIONS FOR CURVED BARS C-1

Appendix D. PLATE THERMAL STRESSES WITH ONE SUPPORT FLOATING D-1

Appendix E. THERMAL ANALYSIS FOR ONE PLATE HOTTER THAN SURROUNDING PLATES E-1

Appendix F. THERMAL STRESSES IN THE LONGITUDINAL DIRECTION OF THE PLATES F-1

Appendix G. THERMAL BUCKLING OF PLATES IN A LONGITUDINAL DIRECTION G-1

LIST OF FIGURES

Figure		Page
1	Pressure coefficient vs Reynolds' number data from lower plate element, plate 55	4
2	Fuel elements	6
3	Three-quarter point section of lower plates (nos. 66, 55, and 44) for the Advanced Neutron Source	7
4	Entrance of lower plates (nos. 66, 55, and 44) for the Advanced Neutron Source	8
5	Three-quarter section of upper plates (nos. 4, 6, and 5) for the Advanced Neutron Source	9
6	Entrance of upper plates (nos. 4, 6, and 5) for the Advanced Neutron Source	10
7	Smissaert's experimental deflection compared to calculated deflection	12
8	Advanced Neutron Source (ANS) lower element plate calculated deflection at the ANS operating velocity of 25 m/s	13
9	Lower element plate calculated stress at Advanced Neutron Source operating velocity of 25 m/s	14
10	Tensile strength of 6061-T0 aluminum as a function of temperature	16
A.1	Involute loads	A-4
B.1	Involute with concentrated load	B-4
C.1	Curved bar loads	C-4
F.1	Free body of longitudinal thermal forces	F-4
G.1	Thermal buckling load	G-4

ACRONYMS AND SYMBOLS

ANS	Advanced Neutron Source
A	cross-sectional area of plates, cross-sectional area of flow, and a buckling constant
a	involute radius and inside radius of a polar element
B	a buckling constant
b	outside radius of a polar element
C_1, C_2	constants
D	flexural rigidity
ds	element of arc length
E	modulus of elasticity
F_{PS}	average plate force in axial (length) direction
F_o	average force in the outside support cylinder in axial (length) direction
F_i	average force in the inside support cylinder in the axial (length) direction
h	flow channel height (thickness)
I	moment of inertia
$\mathbf{l}$	element length
$M, M_{op}, M_F,$ M_o, M_{ip}	moments
m	integer
$N, N_{op}, N_o,$ N_{ip}, N_{oF}, N_l	loads along the element arc direction
N_x	axial plate load
n	exponent
Re	Reynolds' number
r	radius
s	plate width
T	temperature
U	strain energy
V	average flow velocity
$V_{ip}, V_{op}, V_o,$ V_{oF}, V_l, F	loads perpendicular to the element arc
w	out of plane deflection
x, y	coordinates
x_l, y_l	x- or y-coordinate projection of involute plate
α	coefficient of thermal expansion of element
$\Delta p, p$	pressure difference between channels bounding a plate
ΔT	temperature difference
$\delta_F, \delta_{ps},$	

δ_o, δ_i	plate deflections
ϕ, ϕ_l, ϕ_F	involute angle, total involute angle, involute angle to load F
γ	Poison's ratio
μ	dynamic coefficient of viscosity
ρ	coolant mass density
σ	principal stress
θ	polar coordinate

AN ELASTIC EXAMINATION OF THE STRUCTURAL RESPONSE OF THE ADVANCED NEUTRON SOURCE FUEL PLATES

W. F. Swinson
C. R. Luttrell
G. T. Yahr

ABSTRACT

Procedures for evaluating the elastic structural response of the Advanced Neutron Source (ANS) fuel plates to coolant flow and to temperature variations are presented in this report. Calculations are made that predict the maximum deflection and the maximum stress for a representative plate from the upper and from the lower fuel elements.

---

1. INTRODUCTION

A reasonable assessment of any structure starts with knowing what loads are applied. However, this information is not always easily known, as in this case of the Advanced Neutron Source (ANS) fuel plates reacting to the high velocity coolant flow. In addition, the temperature distribution in the plates in response to the coolant flow and to the nuclear reactions is not easily ascertained.

The coolant flow past the ANS fuel plates is highly turbulent. The magnitude of this turbulence is appreciated in noting that the Reynolds' number at transition from laminar to turbulent flow for parallel flat plates is 1,400, while the Reynolds' number for the ANS coolant flow is above 30,000. Highly turbulent flow is characterized as having large amounts of rotational energy, where lumps of mass flow with unsteady motion, and as having numerous swirls and eddies throughout a three-dimensional flow field. Further complications are evident in that flow separation occurring upstream to the plates will create an unpredictable and uneven pressure distribution at the leading edges of the plates, which, in turn, will have a significant effect on the plate response. Finding an analytical model to describe this flow field would be very difficult, if it could be done at all. Analytical models based on classical techniques and experimental data for the ANS plates do not correlate.[1] This lack of correlation is tentatively attributed to the difficulty of developing a continuum model that can account for the difference in rotational energy and the unsteady motion of highly turbulent flow between channels.

Instead of a purely analytical or experimental solution, a combined empirical and analytical solution has been developed and is described herein.

2. PLATE RESPONSE TO COOLANT FLOW

This analysis uses an empirical solution based on experimentation for assigning the flow load to a plate and an analytical solution for predicting elastic response of the plate to this assigned load.

The average pressure in a channel can be predicted reasonably; however, experimental data indicate that it is the pressure difference between channels that is the most significant variable in predicting plate response. These pressure differences between plates are small in comparison to the entering channel pressure, which, in addition to the problems noted above, makes it difficult to model this effect. In experimental fluid mechanics, the drag, and pressure distribution around an immersed body are often related to the pressure coefficient $\left(\frac{\Delta p}{\rho V^2}\right)$ and to the Reynolds' number (Re), $\frac{\rho V h}{\mu}$. Using these two dimensionless terms to relate the pressure difference between two adjacent channels, the following form is taken and examined:

$$\frac{\Delta p}{\rho V^2} = C_1 \left(\frac{\rho V h}{\mu}\right)^n \quad , \tag{1}$$

where

Δp = the pressure difference across a plate,
ρ = mass density of the fluid,
V = average flow velocity,
C_1 = constant of proportionality,
h = channel thickness,
μ = dynamic coefficient of viscosity, and
n = exponential constant.

To help assess the usefulness of Eq. 1, a log-plot of the data from the central plate model of the lower test element is shown in Fig. 1. In addition to the data, two potential curve fits, which will be examined, are illustrated in Fig. 1. The "horizontal line fit" results in the pressure coefficient being independent of the Reynolds' number. The "sloped line fit" results in the pressure coefficient being related to the Reynolds' number. Before examining these two line fits, some comments are offered about the scatter in the data. First, the scatter shown in the data is not uncharacteristic of turbulent flow. The effect of this scatter in the pressure load applied to a plate is attenuated in arriving at the final calculated plate deflection. This effect is readily apparent when it is recalled that, in finding deflection of a beam, one fundamentally starts with the load function (in this case, the pressure load) and integrates four times to find deflection. Each of the integrations is a smoothing operation and tends to attenuate the effect of any scatter in the load function on the calculated deflection. Thus, the effect of the turbulent flow scatter shown in Fig. 1 on the calculated plate deflection is attenuated.

The sloped line fit shown in Fig. 1 was established using the mehtod of least squares. With this function, Eq. 1 becomes

$$\Delta p = 0.040 \rho V^2 \left(\frac{\rho V h}{\mu}\right)^{0.177} \quad . \tag{2}$$

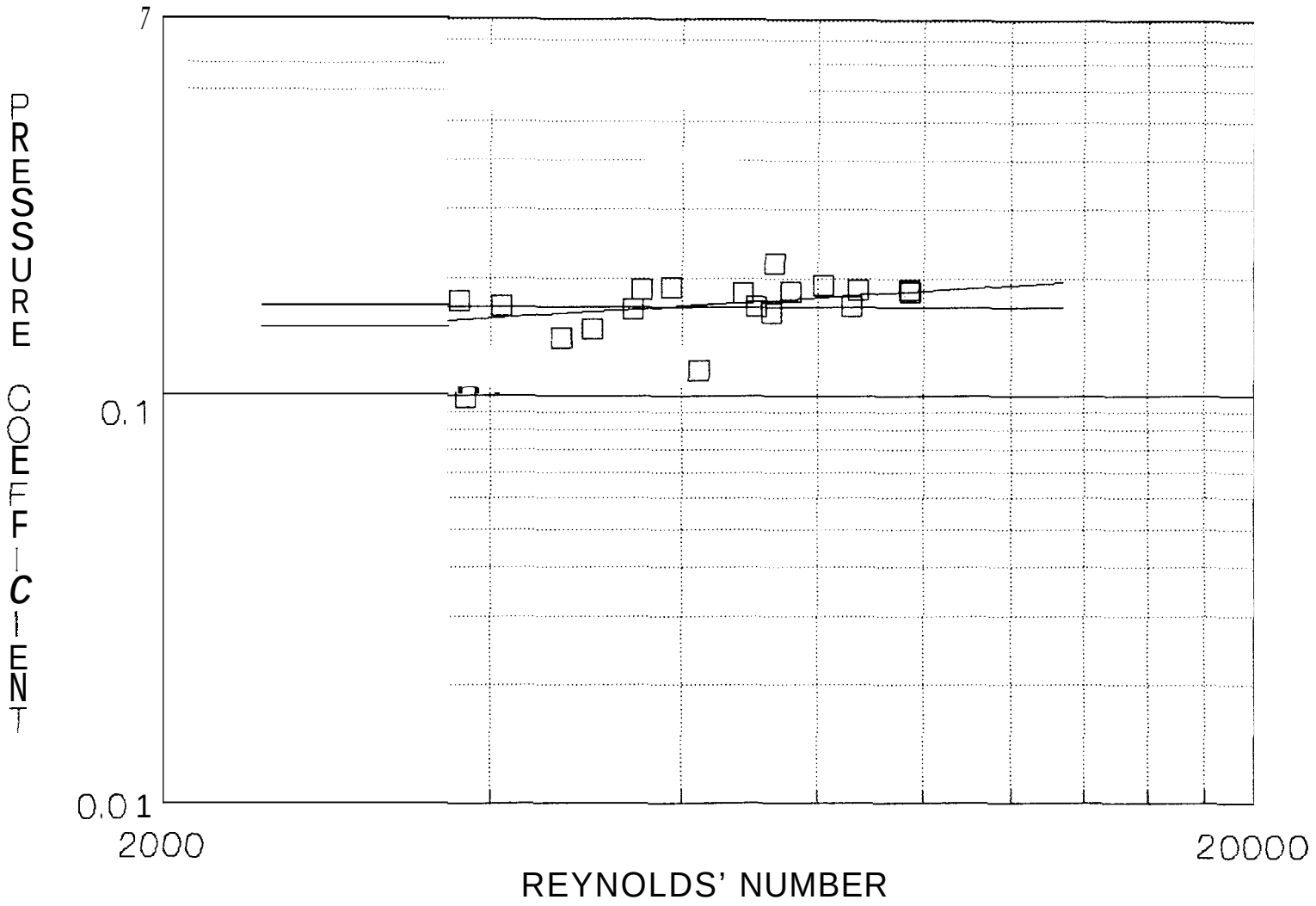

Fig. 1. Pressure coeffiient **vs** Reynolds' number **data** from Iower plate element, plate ***55.***

If the horizontal line of Fig. 1 is used to establish the constants of Eq. 1, the result is

$$\frac{\Delta p}{\rho V^2} = 0.186 \quad . \tag{3}$$

Either Eq. 2 or 3 could be used to determine the load on a plate and then used with a theoretical solution to calculate the deflection. Eq. 3 has the advantage of being slightly more simple to use. On the other side, the correlation coefficient for Eq. 2. is 0.3660 and 0 for Eq. 3. Therefore, on the basis of correlation coefficients, Eq. 2 is preferred.

Another basis for comparing the two equations is to calculate the respective pressure loads at the anticipated operating flow velocity. In performing this calculation, it can be seen that the pressure load determined by Eq. 2 is 35% larger than the pressure load calculated with Eq. 3. From a design viewpoint, the larger pressure load of Eq. 2 is preferred because is gives a more conservative structural design estimate.

A final point for comparison is to note that the channel thickness does not appear as a variable in Eq. 3. Intuitively, one would surmise that the pressure load on a plate for this type of flow is related to the channel thickness, which would give preference to Eq. 2 over Eq. 3. Because of these factors, Eq. 2 is used in the following analyses and comparisons.

An analytical solution for involute plates subjected to pressure loads using energy techniques was developed and is included in Appendices A and B. A finite element analysis gives the sameresult. With the pressure load as predicted by the empirical results of Eq. 2 and the analytical solution of the plate, the maximum deflection of the plate was calculated and is compared with the experimental data. Figure 2 illustrates how the comparisons are shown in Figs. 3 and 4. At a given cross-section, such as entrance or three-quarter, the maximum deflection from three successive plates is shown on the same figure. For further comparison, the zero deflection for each plate is separated by the 1.27-mm channel spacing. With this separation shown, the way in which the channel spacing changes with plate deflection can be seen. The comparisons are made with experimental data taken at the entrance and at the three-quarter point of the lower plates. These two cross-sections had the most significant deflections, and, rather than introduce a longitudinal wave component into Eq. 2 to account for this response, it was more convenient to make comparisons at both cross-sections. The results, from a design viewpoint, seem reasonable for an operating flow velocity of 25 m/s for ANS in that, for some plates, the fit is close, while for others, the fit is conservative.

The next question involves whether Eq. 2 is general or restricted to the geometry of the experiment. Since Eq. 2 was formulated with data from the lower plates, the result is compared with the experimental data from the upper plate models and is illustrated in Figs. 5 and 6. The kind of fit is similar to the comparisons made with the lower plate models, suggesting that, for small geometric changes, Eq. 2 is a reasonable approximation of the applied pressure load. The next comparison is made with plates that are flat instead of involute and with much thicker coolant channels. The data are taken from ref. 2. Data include:

plate dimensions—114.3 × 1.473 × 1143 mm,
polyvinylchloride plastic plate properties—
  elastic modulus = 3309 MPa,
  Poisson's ratio = 0.25,
longitudinal boundaries are clamped, and
channel thickness = 6.426 mm.

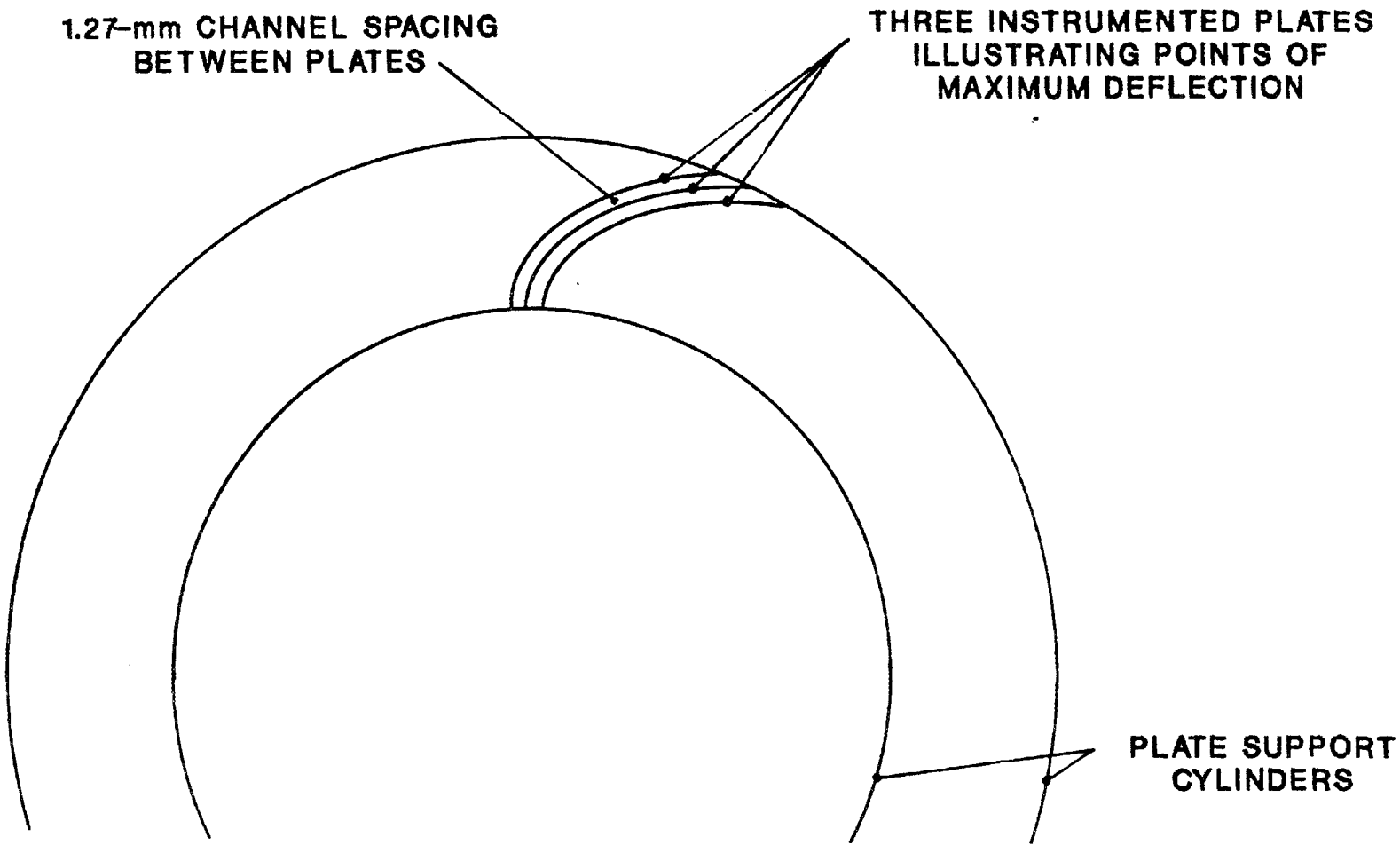

Fig. 2. Reactor cross-section.

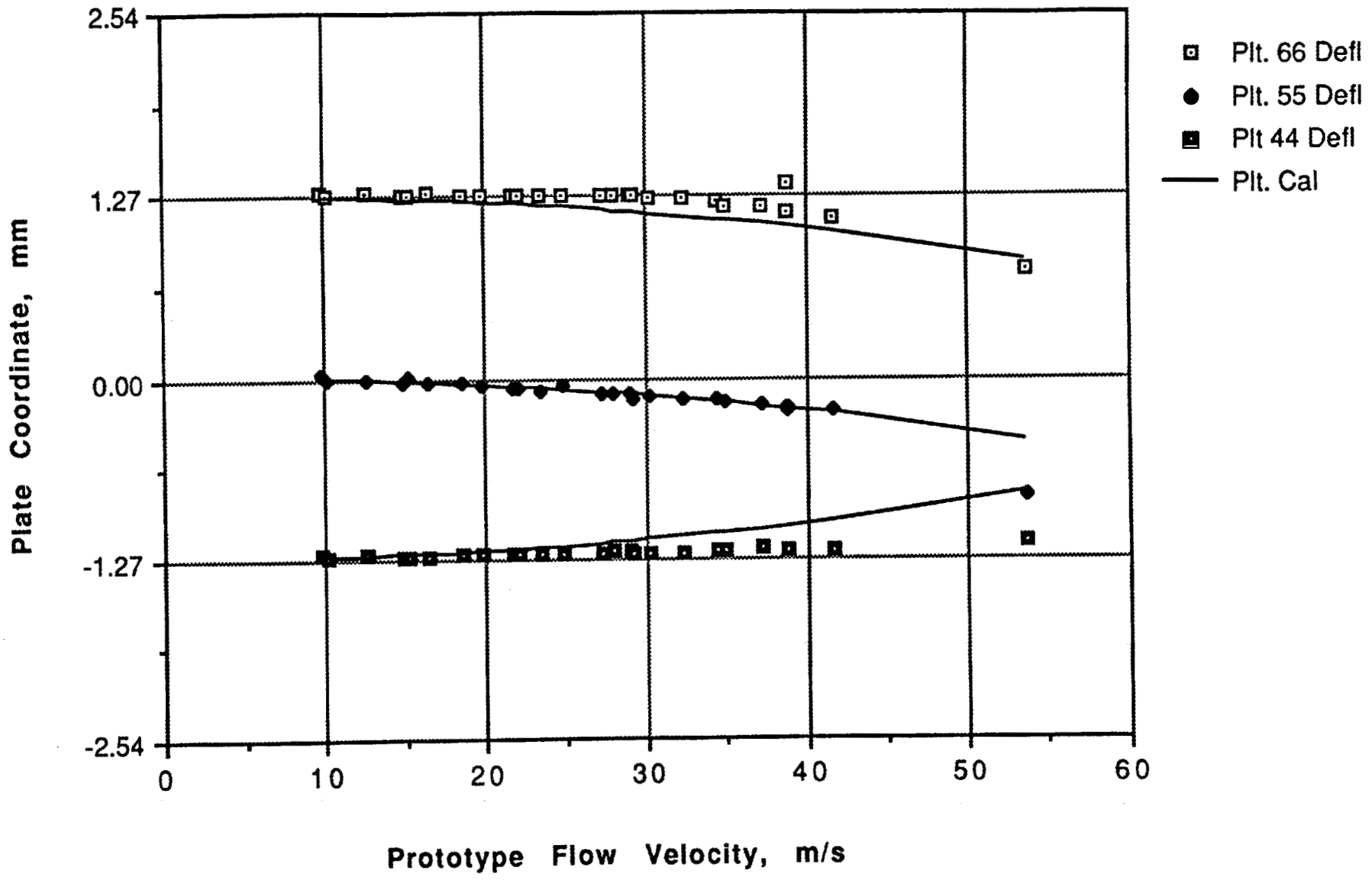

Fig. 3. Three-quarter point section of lower plates (nos. 65, 55, and 44) for the Advanced Neutron Source.

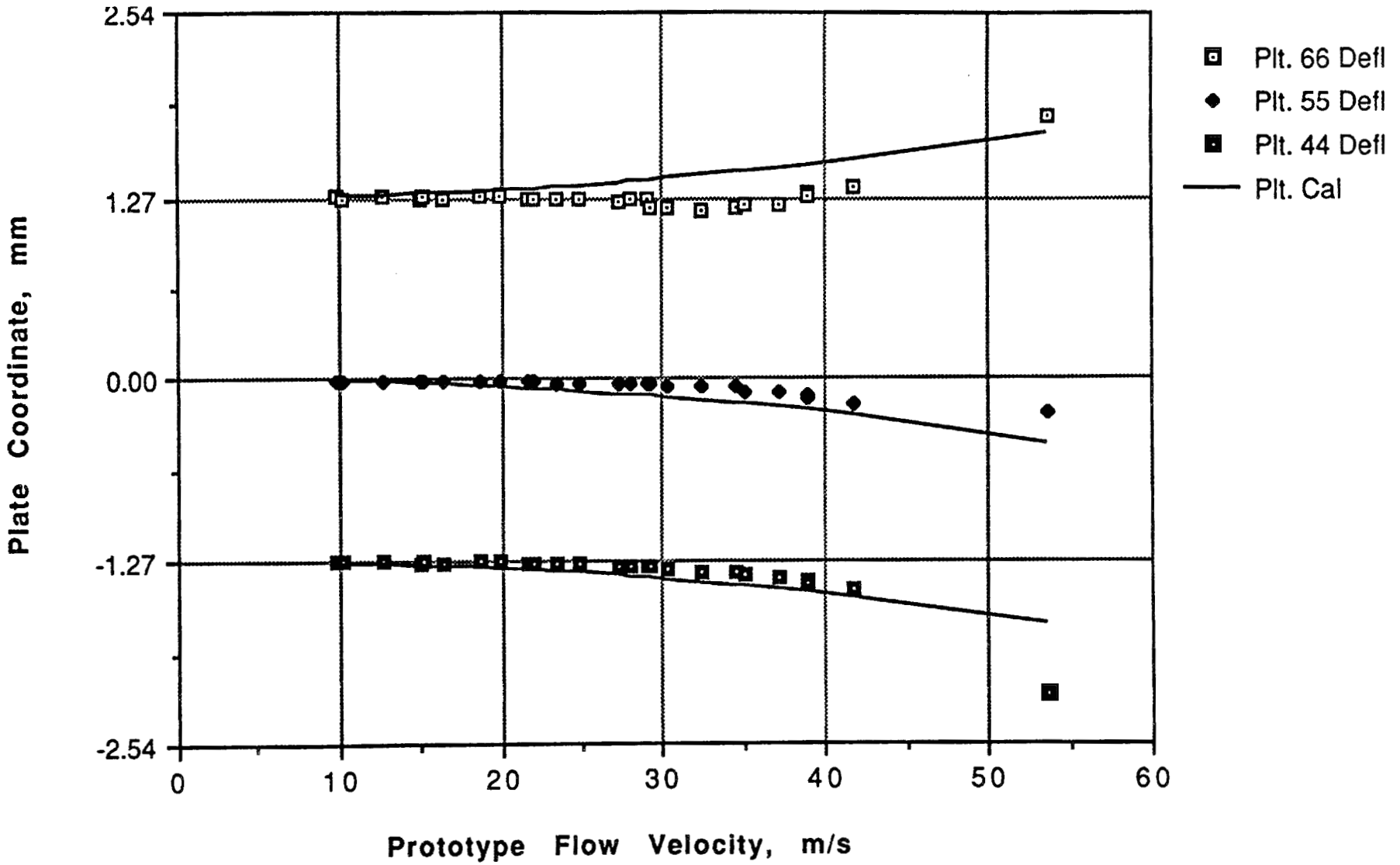

Fig. 4. Entrance of lower plates (nos. 66, 66, and 44) for the Advanced Neutron Source.

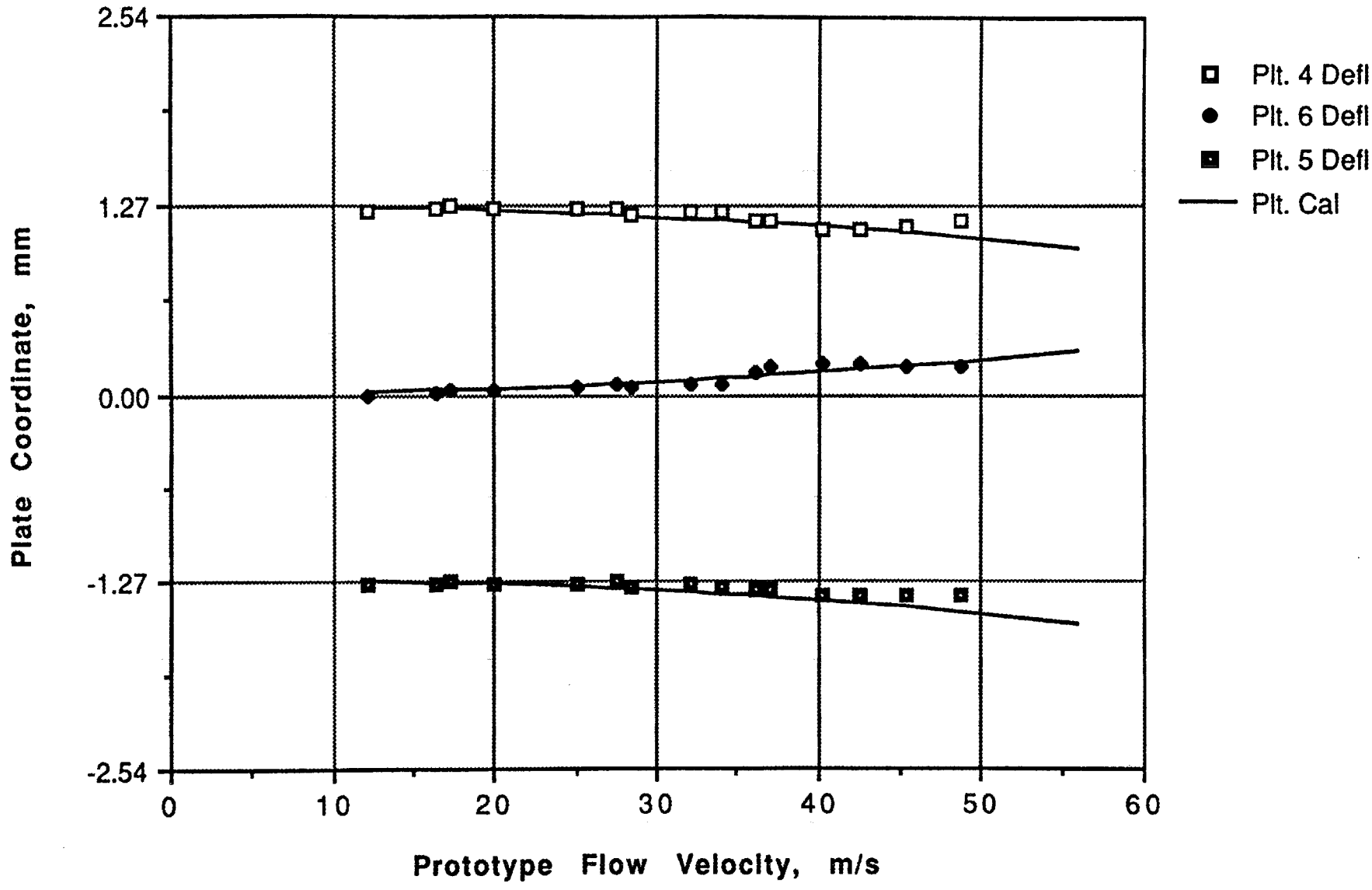

Fig. 5. Three-quarter section of upper plates (nos. 4, 6, and 5) for the Advanced Neutron Source.

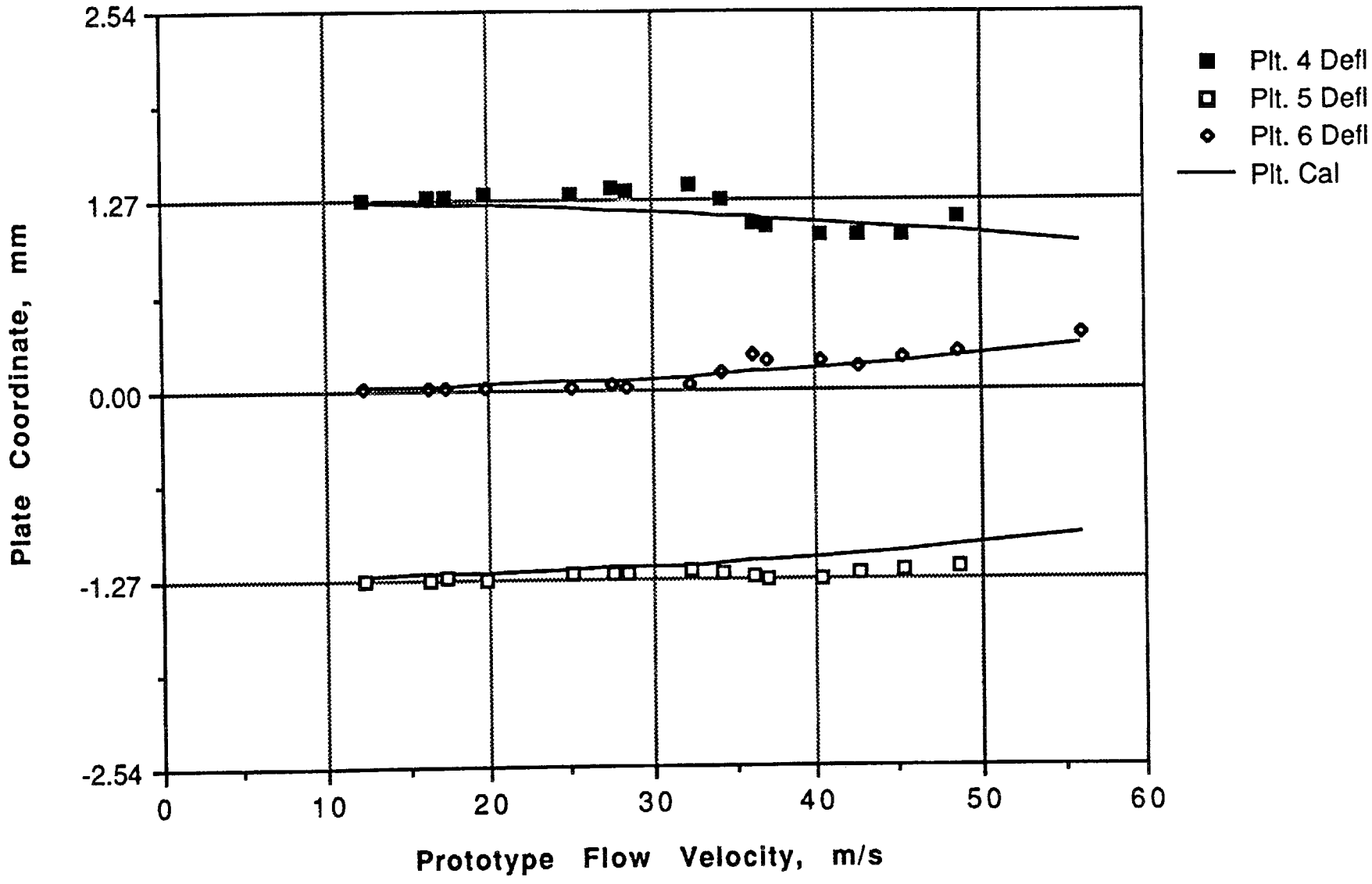

Fig. 6. Entrance of upper plates (nos. 4, 6, and 5) for the Advanced Neutron Source.

The comparison is shown in Fig. 7. The calculated values are lower than the experimental values at low velocities, but are close at higher velocities. It should be noted that the channel height for flat plates is five times more than the channel height for the involute tests.

The overall conclusion is that, for design purposes, the pressure load between two adjacent channels with similar involute geometries can be approximated with Eq. 2. At this point, there are not enough data available to conclude whether Eq. 2 is general or restrictive. It should be noted that the pressure load, as approximated by Eq. 2, is independent of plate properties and would apply just as well to aluminum plates as to epoxy plates.

With the empirical load and the theoretical response of the upper involute plates to this load, the following deflections were calculated at the ANS operating flow velocity (25 m/s):

maximum upper plate deflection = 0.051 mm (0.0020 in.) and
maximum lower plate deflection = 0.104 mm (0.004 in.).

The maximum deflection anticipated for the upper plate resulting from the pressure load is less than 4% of the channel height. The maximum anticipated deflection for the lower plate resulting from the pressure load is less than 8% of the channel height. Neither of these deflection values would be of structural concern in the reactor operation. Fig. 8 is shown to help evaluate the magnitude of this deflection in comparison to the channel height. The lines above and below the abscissa are scaled to represent the channel height of 1.27 mm compared to the plate deflection resulting from the expected pressure load at the operating flow velocity of the ANS.

The largest principal stress in the plates resulting from pressure will occur at the intersection of the plates with the inside support cylinders. The calculated stress along the involute arc for both the concave and convex sides of the lower plate using curved beam theory is illustrated in Fig. 9. A comment is noted relative to beam theory or plate theory. Plate theory uses a plane strain assumption, while the beam theory uses a plane stress assumption. The leading edge of the plate is plane stress, and, since this is one of the higher stressed regions, the more flexible plane stress assumption is used. The radius of curvature for the involute plate at the intersection of the plate with the inside support goes to zero. Theoretically, this zero radius of curvature would produce an infinite stress, but, in practice, the plate cannot be fabricated with a zero radius of curvature. A design decision is needed. In order to get an idea of the stress magnitude involved, it is assumed that the smallest radius of curvature achievable is equal to the plate thickness. If other radii were assumed, the stress numbers, of course, would change. The stress numbers calculated will reflect the assumption used. Appendix C summarizes the procedure used in calculating the stresses. Using the empirical pressure load and the resulting theoretical boundary loads, the largest principal stress magnitude in the upper plate is calculated to be

38.7 MPa (5600 psi) ,

and the largest stress magnitude in the lower plate is

72.1 MPa (10,400 psi) .

Consider what the stress values would be if a different fabricated radius of curvautre was assumed. for the lower plate, as the radius of curvature increases, the largest stress point shifts from the concave side of the plate to the convex side of the plate where the stress components related to N_{op} and M_{op} add (Fig. A.1). The stress magnitude decreases from 72.1 to about 65.0 MPa, where the radius of curvature is 1.75 times the plate thickness, then increases to 73.1 MPa as the radius of curvature approaches infinity. For the upper plate, the geometry was such that the largest stress

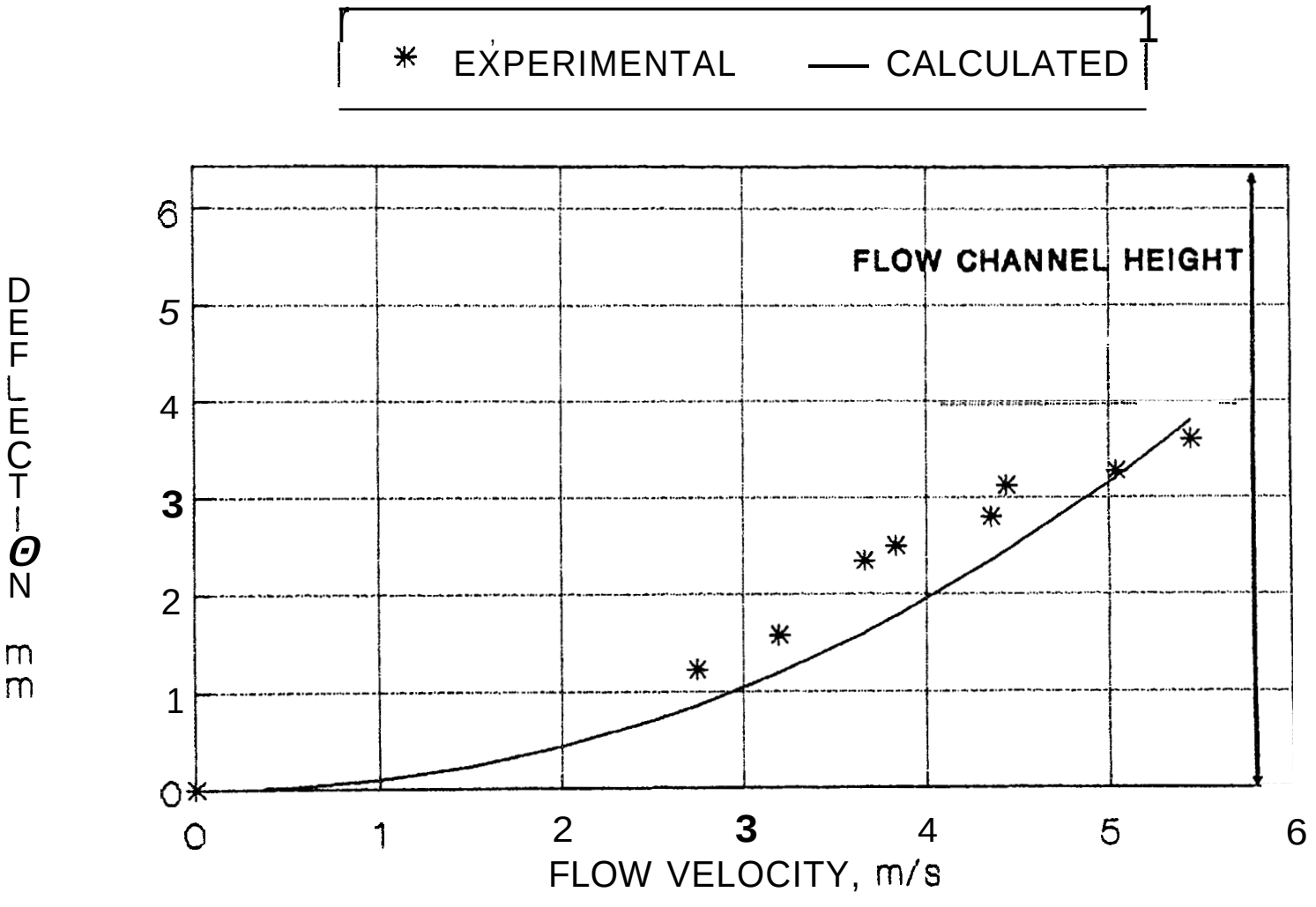

Fig. 7. Smissaert's experimental deflection compared to calculated deflection.

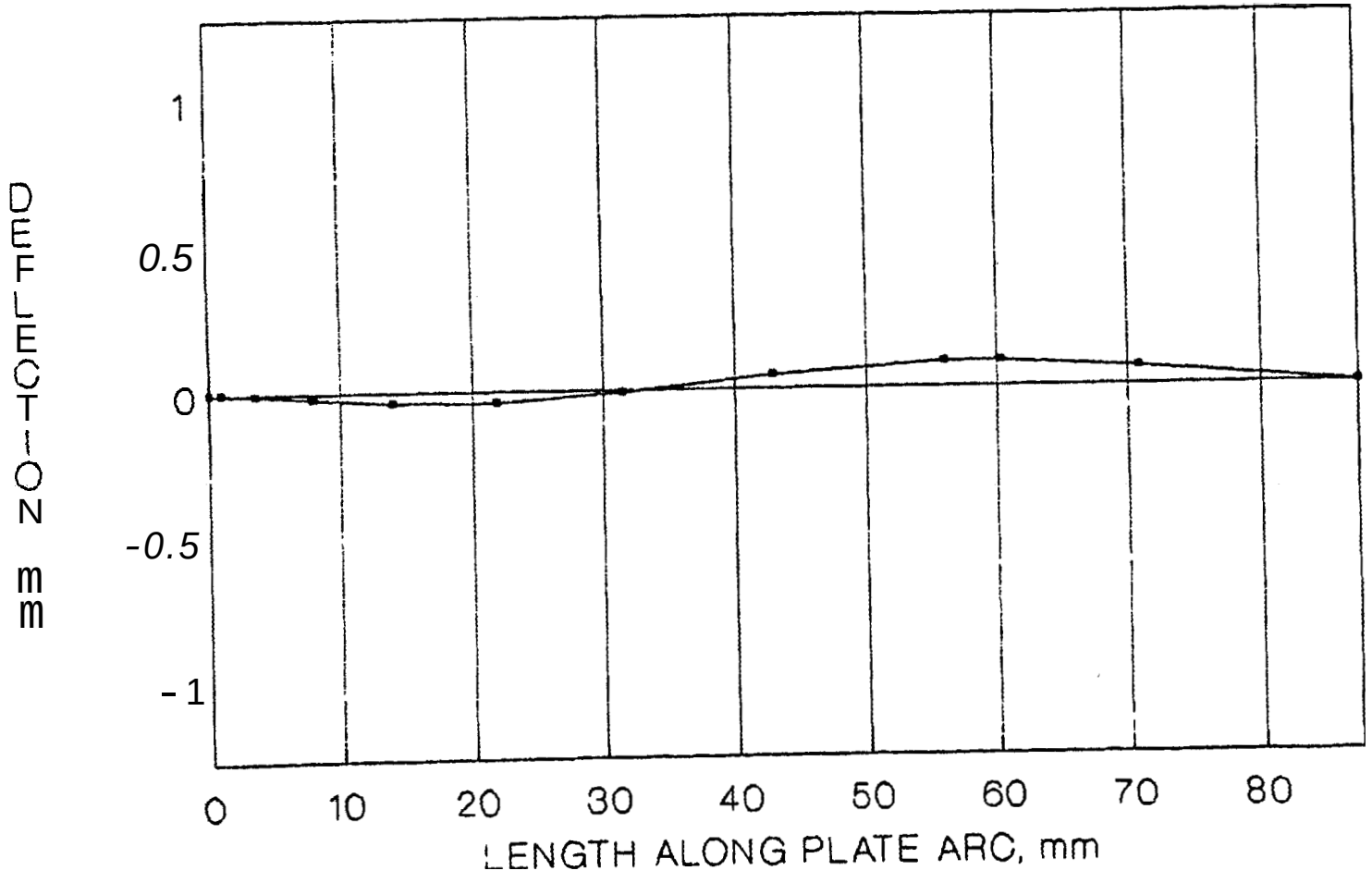

Fig. 8. Advanced Neutron Source lower element plate calculated deflection at ANS operating velocity of 25 m/s.

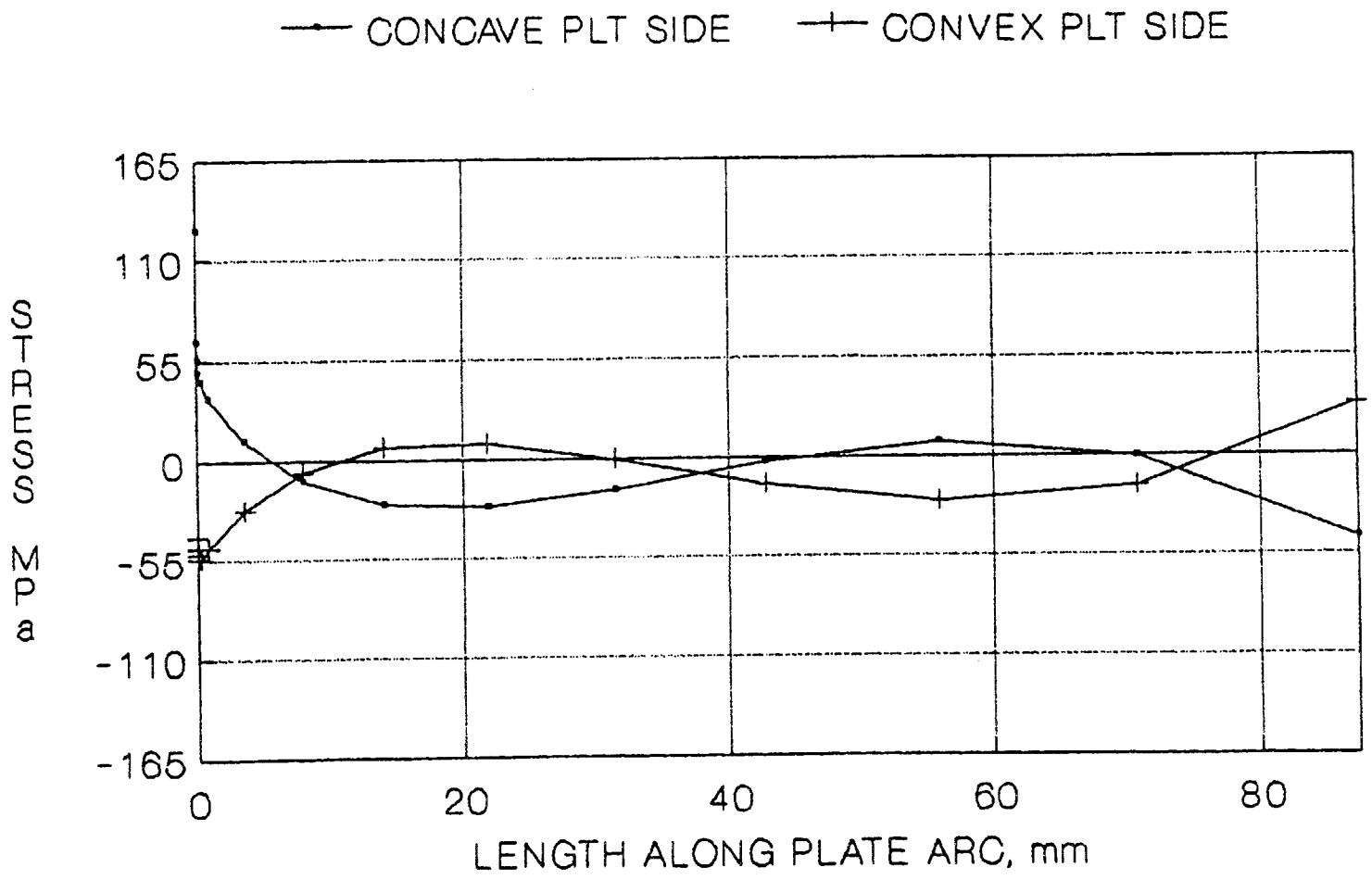

Fig. 9. Lower element plate calculated stress at the Advanced Neutron Source operating velocity of 25 m/s.

point had already shifted to the convex side of the plate with the radius of curvature assumed. Therefore, the stress magnitude for this plate continually increases from 38.7 to 44.8 MPa as the radius of curvature approaches infinity.

The room temperature properties for Aluminum 6061-0 are

yield stress = 55 MPa (8000 psi) ,
tensile strength = 124 MPa (18,000 psi) .

At higher temperatures, the values of these properties are reduced. The stress in the lower plate, with these assumptions, is above yield. If this stress was the only factor in loading the plate, it might be concluded that some local yielding is acceptable; however, there are other contributing factors. There is a stress concentration as a result of the abrupt geometry change at this intersection of the plate with the inside (and outside) support cylinder. A specific number is not well defined, but a multiplier of 1.3 would be a representative number from Peterson's Guide.[4] Residual stress from welding the plates into the side supports will be a factor. Thermal stress as discussed below will be an additional factor. The reduced material properties at higher temperatures may be an additional factor. Figure 10, taken from ref. 5, illustrates the property changes as a function of temperature. The concern with the lower plate is that when all of these factors combine, yielding at the inside support might form a plastic zone sufficient to allow for increased deflection and touching of an adjacent plate.

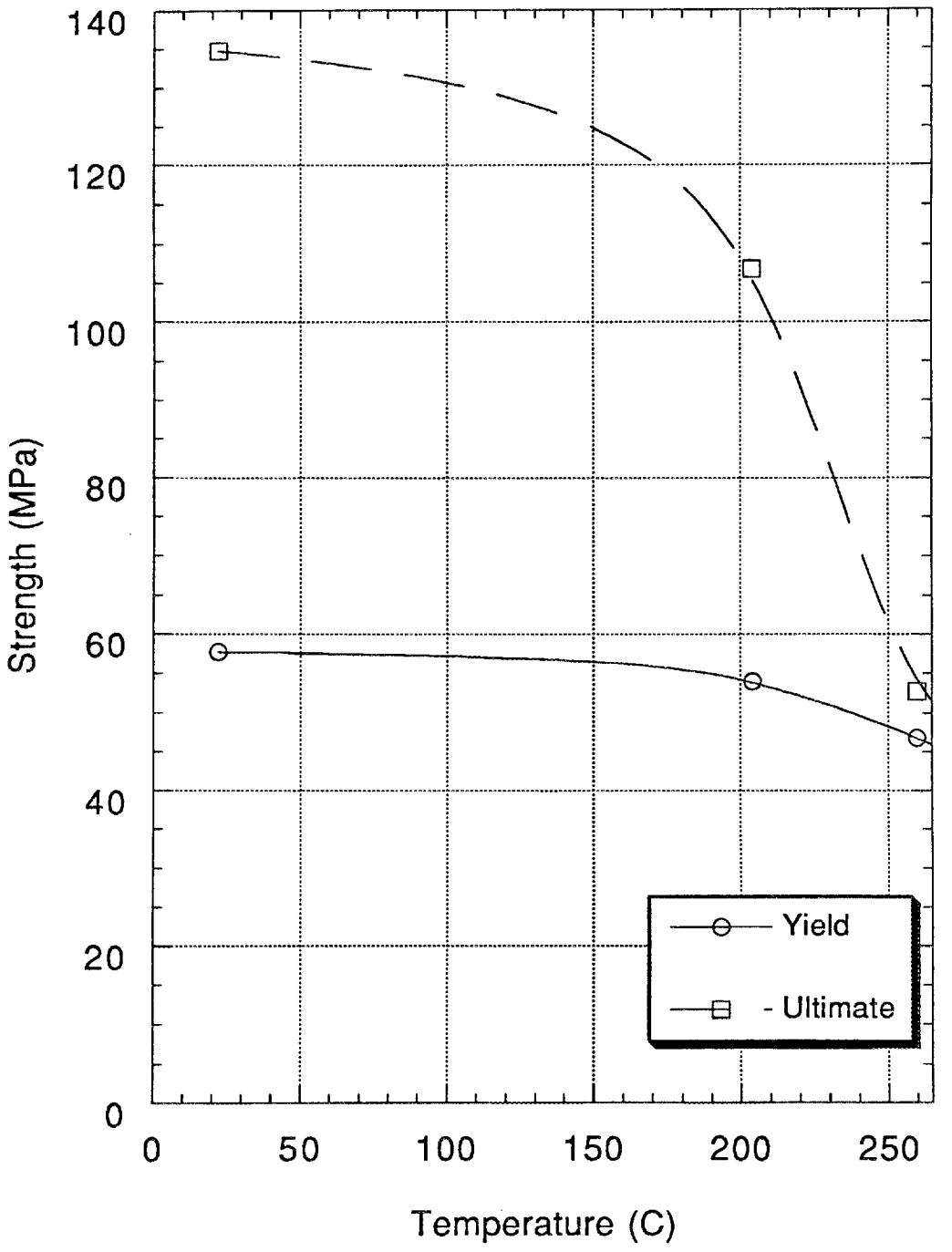

Fig. 10. Tensile strength of Aluminum 6061-T0 as a function of temperature.

3. PLATE RESPONSE TO THERMAL EFFECTS

Because of the reactions in the plates during operation, the plate temperatures will be higher than the side wall support cylinder temperatures. The difference in expansion between the side walls and the plates will induce plate stresses in the longitudinal and transverse direction. In addition, the possibility of the plate buckling must be considered. These effects are discussed below.

1. To minimize thermal stresses along the plate arc length, one support boundary is allowed to float (be free). In analyzing this case, the temperature difference between the side walls and the plates is taken as the average temperature of the plate minus the average temperature of the side walls. The technique for solution is an energy solution and is outlined in Appendix D. A finite element solution yields the same result. Maximum stress values (using curved beam theory) are

   maximum stress upper plate = 0.052 MPa/°C (7.6 psi/°F) and
   maximum stress lower plate = 0.019 MPa/°C (2.7 psi/°F) .

   The average temperature difference that was available for making comparisons did not include conduction heat transfer. The average temperatures are taken at 218°C for the upper plate and 155°C for the lower plate. The side wall temperature is taken as 52°C. These temperature data are based on information supplied by the Thermal Hydraulic Group. Using these values the plate stresses become

   maximum stress upper plate = 15.7 MPa (2300 psi) and
   maximum stress lower plate = 3.5 MPa (500 psi) .

   These values by themselves offer no real concern for plate failure resulting from thermal stresses. However, if these values are superimposed on the stresses resulting from pressure load and then increased by the stress concentration multiplier, failure, based on an elastic analysis, would be expected.

2. The next thermal analysis has to do with the case of one plate becoming hotter than the surrounding plates. For this to occur, one channel would have to be partially blocked to prevent heat removal, or one plate would have to have significantly different fissile loading leading to local power loadings higher than than surrounding plates. The analysis scheme is outlined in Appendix E. Again, using curved beam theory, the induced stresses would be

   maximum stress upper plate = 1.78 MPa/°C (143 psi/°F) and
   maximum stress lower plate = 0.98 MPa/°C (80 psi/°F) .

   If this event is considered to be the only stress producer, then no difficulties would be expected until a single upper plate reached an average temperature of 31°C more than the other structural surroundings or if a single lower plate reached an average temperature of 56°C higher than the other structural surroundings. Since the stresses are expected to be relatively high because of pressure differences in the flow channels, it is imperative that flow not be interrupted and that the heat load from plate to plate be essentially the same.

3. This analysis has to do with the stresses in the longitudinal direction caused by the support cylinders being at a different temperature from the plates. The analysis for this case is outlined in Appendix F. The average longitudinal stresses in the plates are calculated as

   upper plate stress = –0.510 MPa/°C (–41.1 psi/°F) and
   lower plate stress = –0.477 MPa/°C (–38.5 psi/°F) .

   Using the available temperature difference, as noted above, the stresses are calculated as

   upper plate stress = –85 MPa (–12,330 psi) and
   lower plate stress = –49.1 MPa (–7123 psi) .

   The stress in the upper plate is much larger than the 55 MPa yield stress property for Aluminum 6061-0. With a plate in yield in the longitudinal direction resulting from thermal effects and with some regions in yield in the transverse direction resulting from pressure and thermal effects, the formation of plastic hinges would be expected. This formation is a concern because characteristics of plastic hinges are large strains (and deformation) with little change in load. Thus, the undesirable possibility of plates touching has to be considered.

4. The potential of the plate buckling as a result of the thermal loading is considered. First, thermal expansion of the plate along the arc length (transverse direction) of the involute is not completely restrained, since one of the support cylinders is free to rotate. This rotation of one of the side walls as noted in part one of this section will assist in keeping the thermal loads in the transverse direction small and prevent buckling. Thermal buckling of the plate in the longitudinal direction is considered in this part of the analysis. It is noted for emphasis that one of the early failures of an engineering test reactor plate had the appearance of a thermally induced longitudinal buckling failure.[6] The assumptions and development of this analysis are outlined in Appendix G. The calculations indicate that longitudinal buckling would occur if the average temperature difference between the plates and side walls were

   upper plate longitudinal buckling temperature = 284°C (512°F) and
   lower plate longitudinal buckling temperature = 197°C (354°F) .

   When this potential for buckling is considered along with the fact that the assumptions made produce some conservatism, there does not appear to be a longitudinal thermal buckling problem. Also, the yielding as noted in the preceding analysis would occur before this buckling state is reached.

4. CONCLUSIONS AND RECOMMENDATIONS

This analysis is an elastic analysis. In such an analysis, any structural relief occurring because of creep or yield is taken as an unknown factor of safety or built-in conservatism. In assessing the following conclusions and recommendations, one needs to be aware of the "elastic design school of thought" used.

1. With the present design, the pressure load on the plates resulting from flow at the operating flow velocity of the ANS is projected to be a potential plate failure mechanism. The pressure load itself will produce some yielding in the plates, and, when this is combined with a stress concentration factor, some thermal stress, some residual stress, and some material property degradation excessive plate deformation is possible. This possibility is further enhanced by the flow pattern being generated upstream. The core latch mechanism constricts and redirects the flow for one set of plates and the transuranium production rods will have a significant effect on the flow pattern entering the other set of plates. The wakes, vortices, and eddies generated by these obstructions have the potential of causing larger pressure differences (pressure loads) than would be predicted by Eq. 2 and result in even higher stresses. Such an effect was noted and reported in ref. 1. It is recommended that changes be made to alleviate this stress problem. For example, calculations show that a plate with a constant, relatively large (say, 100 mm) radius of curvature will have less stress.

2. The stresses in the longitudinal sense caused by an average temperature difference of 166°C for the upper plates and 103°C for the lower plates between the side walls and the plates would cause plate stresses to be well in the yield range. Changing the plate configuration as noted above would not alleviate this stress problem. Including conduction in arriving at the sidewall temperature should reduce the temperature difference. If this factor does not reduce the calculated temperature difference, but, if it is indeed too high, then some engineering solution, could be considered to resolve this stress problem.

5. REFERENCES

1. W. F. Swinson et al., *Fuel Plate Stability Experiments and Analysis for the Advanced Neutron Source*, ORNL/TM-12353, Martin Marietta Energy Systems, Inc., Oak Ridge Natl. Lab., May 1993.

2. G. E. Smissaert, "Static and Dynamic Hydro-Elastic Instabilities in MTR-Type Fuel Elements. Part I. Introduction and Experimental Investigation," *Nucl. Eng. Design* **7**, 535–546 (1968).

3. R. D. Groninger and J. J. Kane, "Flow Induced Deflections of Parallel Flat Plates," *Nucl. Sci. Eng.* **16**, 218 (1963).

4. R. E. Peterson, *Stress Concentration Factors*, John Wiley and Sons, New York, 1974.

5. W. R. Martin and J. R. Weir, *Mechanical Properties of X8001 and 6061 Aluminum Alloys and Aluminum-Base Fuel Dispersion at Elevated Temperatures*, ORNL-3557, Oak Ridge Natl. Lab., Oak Ridge, Tennessee, February 1964.

6. R. G. Beck, E. S. Brown, and J. H. Rainwater, *ETR Core Hydraulics*, IDO-16464, Phillips Petroleum Company, Idaho Operations Office, U.S. Atomic Energy Commission, September 1958.

Appendix A

INVOLUTE BOUNDARY LOADS WITH ENERGY TECHNIQUES

Appendix A. INVOLUTE BOUNDARY LOADS WITH ENERGY TECHNIQUES

Referencing the notation of Fig. A.1, the equations of an involute are

$$
\begin{gathered}
a\phi = \left(r^2 - a^2\right)^{1/2} , \\
ds = a\phi \, d\phi , \\
x = a(S\phi - \phi \, C\phi) , \\
y = a(C\phi + \phi \;\; S\phi - 1) ; \\
\text{where } S\phi \text{ and } C\phi \text{ mean sine } \phi \text{ and cosine } \phi, \\
ds = \text{element of arc length.}
\end{gathered}
\tag{A.1}
$$

The values of V_{op}, M_{op}, and N_{op} can be found using energy techniques. The values of M_{lp}, N_{lp}, and V_{lp} can be found from equilibrium. The moment and derivatives at any section can be expressed from equilibrium as

$$
\begin{gathered}
M = M_{op} + N_{op} a(S\phi - \phi \;\; C\phi) + V_{op} a(1 - C\phi - \phi \;\; S\phi) + pa^2\left(1 + \frac{\phi^2}{2} - \;\; C\phi - \phi \;\; S\phi\right) , \\
\frac{\partial M}{\partial M_{op}} = 1 , \\
\frac{\partial M}{\partial N_{op}} = a(S\phi - \phi \quad C\phi) , \\
\frac{\partial M}{\partial V_{op}} = a(1 - C\phi - \phi \;\; S\phi) \; .
\end{gathered}
\tag{A.2}
$$

The axial load and its derivatives are

$$
\begin{gathered}
N = V_{op} \; S\phi + \mathrm{N}_{op} \; C\phi - pa(\phi - S\phi) , \\
\frac{\partial N}{\partial M_{op}} = 0 , \\
\frac{\partial N}{\partial N_{op}} = C\phi ,
\end{gathered}
\tag{A.3}
$$

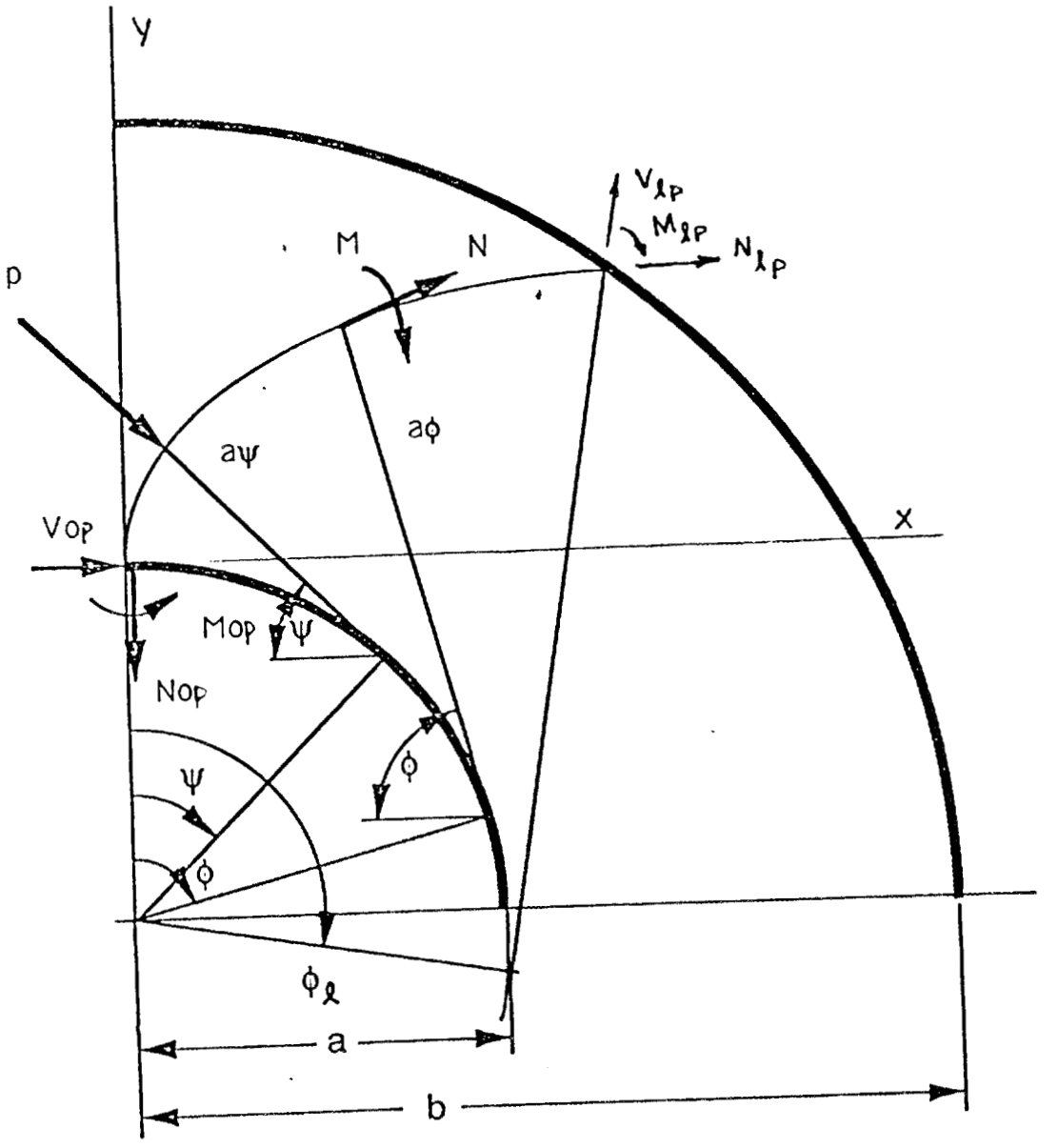

Fig. A.1. Involute loads.

$$\frac{\partial N}{\partial V_{op}} = S\phi \ .$$

Using strain energy, U, and Castigliano's theorem, the change in slope at the origin as load is applied is zero and can be expressed as

$$\frac{\partial U}{\partial M_o} = 0 = \int_0^{\phi_l} \frac{M}{EI} \frac{\partial M}{\partial M_o} a\phi \, d\phi \ . \tag{A.4}$$

The deflection of the involute beam at the origin in the direction of N_o as load is applied is also zero and can be expressed as

$$\frac{\partial U}{\partial N_o} = 0 = \int_0^{\phi_l} \frac{M}{EI} \frac{\partial M}{\partial N_o} a\phi \, d\phi + \int_0^{\phi_l} \frac{N}{AE} \frac{\partial N}{\partial N_o} a\phi \, d\phi \ , \tag{A.5}$$

and the deflection of the involute beam at the origin in the direction of V_o as load is applied is zero and can be expressed as

$$\frac{\partial U}{\partial V_o} = 0 = \int_0^{\phi_l} \frac{M}{EI} \frac{\partial M}{\partial V_o} a\phi \, d\phi + \int_0^{\phi_l} \frac{N}{AE} \frac{\partial N}{\partial V_o} a\phi \, d\phi \ . \tag{A.6}$$

When Eqs. A.4, A.5, and A.6 are expanded by inserting Eqs. A.2 and A.3, the results are three equations and three unknowns, which can be used to solve for M_o, V_o, N_o. In setting up Eqs. A.4, A.5, and A.6 for solution, Table A.1, which is an integral table, was convenient.

Table A.1. Integral table.

$$\int_0^{\phi_\ell} \phi d\phi = \frac{\phi_\ell^2}{2}$$

$$\int_0^{\phi_\ell} \phi s\phi d\phi = s\phi_\ell - \phi_\ell c\phi_\ell$$

$$\int_0^{\phi_\ell} \phi c\phi d\phi = c\phi_\ell + \phi_\ell s\phi_\ell - 1$$

$$\int_0^{\phi_\ell} \phi^2 s\phi d\phi = 2\phi_\ell s\phi_\ell - (\phi^2{}_\ell - 2)c\phi_\ell - 2$$

$$\int_0^{\phi_\ell} \phi^2 c\phi d\phi = 2\phi_\ell c\phi_\ell + (\phi^2{}_\ell - 2)s\phi_\ell$$

$$\int_0^{\phi_\ell} \phi s^2\phi d\phi = \frac{\phi_\ell^2}{4} - \frac{\phi_\ell s2\phi_\ell}{4} - \frac{c2\phi_\ell}{8} + \frac{1}{8}$$

$$\int_0^{\phi_\ell} \phi s\phi c\phi d\phi = \frac{s2\phi_\ell}{8} - \frac{\phi_\ell c2\phi_\ell}{4}$$

$$\int_0^{\phi_\ell} \phi c^2\phi d\phi = \frac{\phi_\ell^2}{4} + \frac{\phi_\ell s2\phi_\ell}{4} + \frac{c2\phi_\ell}{8} - \frac{1}{8}$$

$$\int_0^{\phi_\ell} \phi^2 s^2\phi d\phi = \frac{\phi_\ell^3}{6} - \left(\frac{\phi_\ell^2}{4} - \frac{1}{8}\right)s2\phi_\ell - \frac{\phi_\ell c2\phi_\ell}{4}$$

$$\int_0^{\phi_\ell} \phi^2 s\phi c\phi d\phi = \frac{\phi_\ell}{4}s2\phi_\ell - \left(\frac{\phi_\ell^2}{4} - \frac{1}{8}\right)c2\phi_\ell - \frac{1}{8}$$

$$\int_0^{\phi_\ell} \phi^2 c^2\phi d\phi = \frac{\phi_\ell^3}{6} + \left(\frac{\phi_\ell^2}{4} - \frac{1}{8}\right)s2\phi_\ell + \frac{\phi_\ell}{4}c2\phi_\ell$$

$$\int_0^{\phi_\ell} \phi^3 s^2\phi d\phi = \frac{\phi_\ell^4}{8} - \frac{\phi_\ell^3 s2\phi_\ell}{4} - \frac{3}{8}\phi_\ell^2 c2\phi_\ell + \frac{3}{8}\phi_\ell s2\phi_\ell + \frac{3}{16}c2\phi_\ell - \frac{3}{16}$$

$$\int_0^{\phi_\ell} \phi^3 s\phi c\phi d\phi = \frac{-\phi_\ell^3}{4}c2\phi_\ell + \frac{3}{8}\phi_\ell^2 s2\phi_\ell + \frac{3}{8}\phi_\ell c2\phi_\ell - \frac{3}{16}s2\phi_\ell$$

$$\int_0^{\phi_\ell} \phi^3 c^2\phi d\phi = \frac{\phi_\ell^4}{8} + \frac{\phi_\ell^3}{4}s2\phi_\ell + \frac{3}{8}\phi_\ell^2 c2\phi_\ell - \frac{3}{8}\phi_\ell s2\phi_\ell - \frac{3}{16}c2\phi_\ell + \frac{3}{16}$$

$$\int_0^{\phi_\ell} \phi^3 s\phi d\phi = (3\phi_\ell^2 - 6)s\phi_\ell - (\phi_\ell^3 - 6\phi_\ell)c\phi_\ell$$

$$\int_0^{\phi_\ell} \phi^3 c\phi d\phi = (3\phi_\ell^2 - 6)c\phi_\ell + (\phi_\ell^3 - 6\phi_\ell)s\phi_\ell + 6$$

$$\int_0^{\phi_\ell} \phi^4 s\phi d\phi = -\phi_\ell^4 c\phi_\ell + (12\phi_\ell^2 - 24)c\phi_\ell + (4\phi_\ell^3 - 24\phi_\ell)s\phi_\ell + 24$$

$$\int_0^{\phi_\ell} \phi^4 c\phi d\phi = \phi_\ell^4 s\phi_\ell + (-12\phi_\ell^2 + 24)s\phi_\ell + (4\phi_\ell^3 - 24\phi_\ell)c\phi_\ell$$

Appendix B

INVOLUTE DEFLECTION USING THE DUMMY-LOAD TECHNIQUE

Appendix B. INVOLUTE DEFLECTION USING THE DUMMY-LOAD TECHNIQUE

If it is desirable to know the deflection at some location, for example, ϕ_F on the involute (Fig. B.1), a dummy load F can be applied at the point and the deflection evaluated using energy techniques, such that

$$\delta_F = \int_0^{\phi_F} \frac{M}{EI}\frac{\partial M}{\partial F} a\phi d\phi + \int_{\phi_F}^{\phi_\ell} \frac{M}{EI}\frac{\partial M}{\partial F} a\phi d\phi + \int_0^{\phi_F} \frac{N}{AE}\frac{\partial N}{\partial F} a\phi d\phi + \int_{\phi_F}^{\phi_\ell} \frac{N}{AE}\frac{\partial N}{\partial F} a\phi d\phi \ , \tag{B.1}$$

where M and N are the same as in Eqs. A.2 and A.3.

To evaluate $\frac{\partial M}{\partial F}$ and $\frac{\partial N}{\partial F}$, the dummy-load technique requires the solution for M_{oF}, N_{oF} and V_{oF} shown in Fig. B.1 with $F = 1$. The approach is similar to the solution shown in Appendix A. The moment equation and axial load equation for an involute with a concentrated force, F, applied are

$$\begin{aligned} M_F &= M_{oF} + N_{oF}a(S\phi - \phi C\phi) + V_{oF}a(1 - c\phi - \phi s\phi) \\ &+ \left\{ Fa\left[s\phi_F\left(s\phi - \phi c\phi - \frac{x_F}{a}\right) + c\phi_F\left(c\phi + \phi s\phi - 1 - \frac{y_F}{a}\right)\right]\right\} \\ N_F &= N_{oF}c\phi + V_{oF}s\phi + \left\{F(s\phi_F c\phi - c\phi_F s\phi)\right\} \ , \end{aligned} \tag{B.2}$$

where $\{\} = 0$, if $0 \le \phi \le \phi_F$ and $\{\} = ()$ for $\phi_F \le \phi \le \phi_\ell$. Again, because of the boundary conditions of slope and deflection being zero at the origin, three equations can be generated through energy techniques for finding M_{oF}, N_{oF}, and V_{oF} with $F = 1$,

$$\frac{\partial U}{\partial M_{oF}} = 0 = \int_0^{\phi_F} \frac{M_F}{EI}\frac{\partial M_F}{\partial M_{oF}} a\phi d\phi + \int_{\phi_F}^{\phi_\ell} \frac{M_F}{EI}\frac{\partial M_F}{\partial M_{oF}} a\phi d\phi \ , \tag{B.3}$$

$$\begin{aligned} \frac{\partial U}{\partial N_{oF}} = 0 = &\int_0^{\phi_F} \frac{M_F}{EI}\frac{\partial M_F}{\partial N_{oF}} a\phi d\phi + \int_{\phi_F}^{\phi_\ell} \frac{M_F}{EI}\frac{\partial M_F}{\partial N_{oF}} a\phi d\phi \\ &+ \int_0^{\phi_F} \frac{N_F}{AE}\frac{\partial N_F}{\partial N_{oF}} a\phi d\phi + \int_{\phi_F}^{\phi_\ell} \frac{N_F}{AE}\frac{\partial N_F}{\partial N_{oF}} a\phi d\phi \end{aligned} \ , \tag{B.4}$$

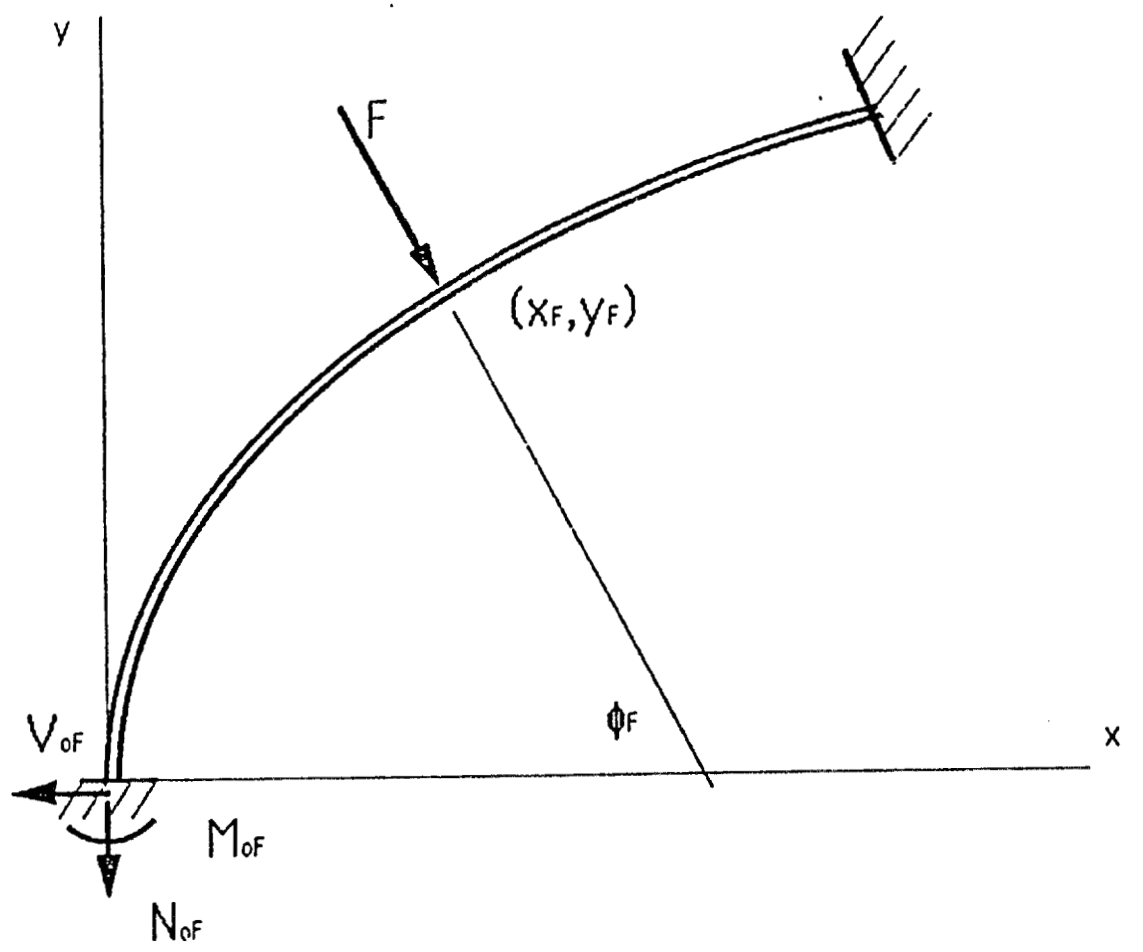

Fig. B.1. Involute with concentrated load.

$$\frac{\partial U}{\partial V_{oF}} = 0 = \int_0^{\phi_F} \frac{M_F}{EI}\frac{\partial M_F}{\partial V_{oF}} a\phi d\phi + \int_{\phi_F}^{\phi_t} \frac{M_F}{EI}\frac{\partial M_F}{\partial V_{oF}} a\phi d\phi + \int_0^{\phi_F} \frac{N_F}{AE}\frac{\partial N_F}{\partial V_{oF}} a\phi d\phi + \int_{\phi_F}^{\phi_t} \frac{N_F}{AE}\frac{\partial N_F}{\partial V_{oF}} a\phi d\phi \quad . \tag{B.5}$$

Equations B.3, B.4, and B.5 can be solved for M_{oF}, N_{oF}, and V_{oF}. Now, having M_{oF}, N_{oF}, and V_{oF}, $\frac{\partial M}{\partial F}$ of Eq. B.1 can be found as

$$\frac{\partial M}{\partial F} = (M_F)_{F=1} = M_{oF} + N_{oF}a(s\phi - \phi c\phi) + V_{oF}a(1 - c\phi - \phi s\phi) + \left\{ a\left[s\phi_F\left(s\phi - \phi c\phi - \frac{x_F}{a} \right) + c\phi_F\left(c\phi + \phi s\phi - 1 - \frac{y_F}{a} \right) \right] \right\} , \tag{B.6}$$

and $\frac{\partial N}{\partial F}$ of Eq. (B-1) is

$$\frac{\partial N}{\partial F} = (N_F)_{F=1} = N_{oF}c\phi - V_{oF}s\phi + \{ s\phi_F c\phi - c\phi_F s\phi \} \ . \tag{B.7}$$

Finally, Eq. B.1 can be expanded using Eqs. B.6 and B.7 for the partial derivative expressions and Eqs. A.2 and A.3 for the moment and axial load expressions. The integral table, Table A.1, is again helpful in solving Eq. B.1.

Appendix C

STRESS CALCULATIONS FOR CURVED BARS

Appendix C: STRESS CALCULATIONS FOR CURVED BARS*

Discussions on finding stresses in curved bars can be found in most elasticity treatments and the results of one treatment are summarized below. The circumferential stress resulting from an applied moment is given as

$$\sigma = \frac{4M}{N_1}\left(- \frac{a^2b^2}{r^2} \ \ell n \frac{b}{a} + b^2 \ell n \frac{r}{b} + a^2 \ell n \frac{a}{r} + b^2 - a^2 \right), \tag{C.1}$$

where (see Fig. C.1)

a = inside radius of bar,
b = outside radius of bar,
r = radius to any point,
M = applied moment per unit width, and
$N_1 = (b^2 - a^2)^2 - 4a^2b^2 \left(\ell n \frac{b}{a} \right)^2$.

Superimposed on the bending stress is the stress

$$\sigma = \left(\frac{N}{A} \right), \tag{C.2}$$

where

N = load per unit width applied to the θ surfaces, and
A = θ surface area for a unit width.

*The material in this appendix is drawn from S. Timoshenko and J. N. Goodier, *Theory of Elasticity*, third edition, McGraw-Hill Book Company, Inc., New York, 1970.

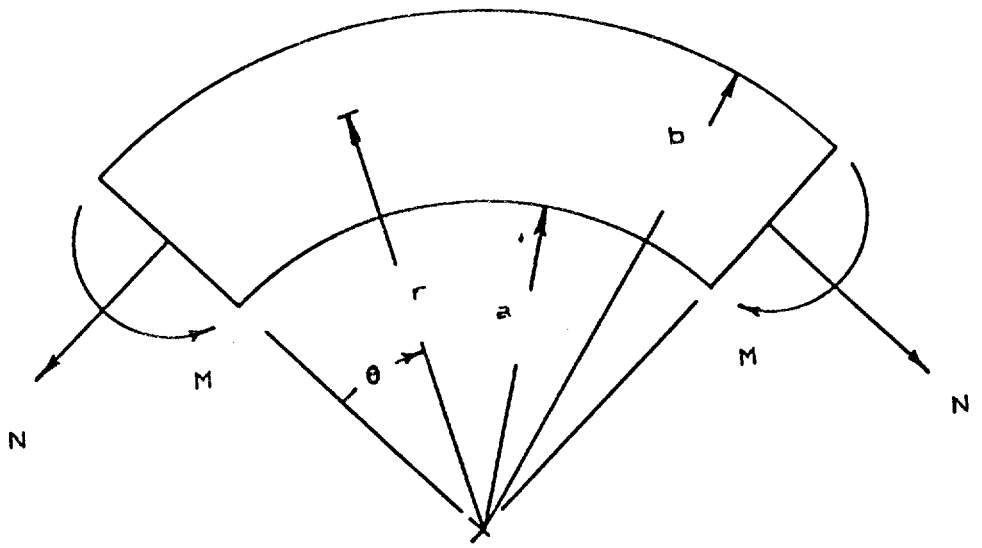

Fig. C.1. Curved bar loads.

Appendix D

PLATE THERMAL STRESSES WITH ONE SUPPORT FLOATING

Appendix D. PLATE THERMAL STRESSES WITH ONE SUPPORT FLOATING

Plate stresses, which result from the plate being at one temperature and the support boundaries at a different temperature, are calculated using energy techniques. The boundary conditions are assumed to be such that one support cylinder can rotate relative to the other cylinder. The distance between channels remains constant, which assumes that all deformation is in the plates, although, in reality, the cylinders do deform and reduce the stresses. Reference Fig. A.1, let $p = 0$, and assume the inner support is free to rotate. First, let the plate expand in the N_o direction by

$$\alpha\, y_\ell \Delta T\,,$$

where

α = coefficient of thermal expansion,
y_ℓ = the y-coordinate projection of the plate,
ΔT = temperature difference between plate and side walls.

Now apply the inner boundary and in effect remove the plate displacement in the N_o direction, thus, Eq. (A.5) can be expressed as

$$\frac{\partial U}{\partial N_o} = -\alpha y_\ell \Delta T = \int_0^{\phi_\ell} \frac{M}{EI}\frac{\partial M}{\partial N_o} a\phi d\phi + \int_0^{\phi_\ell} \frac{N}{AE}\frac{\partial N}{\partial N_o}\phi d\phi\,. \tag{D.1}$$

The plate deflection in the tangential direction can be expressed in terms of rotation, $\frac{\partial U}{\partial M_o}$, or displacement, $\frac{\partial U}{\partial V_o}$, thus, Eqs. A.4 and A.6 are related as

$$-a\int_0^{\phi_\ell} \frac{M}{EI}\frac{\partial M}{\partial M_o} a\phi d\phi = \int_0^{\phi_\ell} \frac{M}{EI}\frac{\partial M}{\partial V_o} a\phi d\phi + \int_0^{\phi_\ell} \frac{N}{AE}\frac{\partial N}{\partial V_o} a\phi d\phi\,. \tag{D.2}$$

From equilibrium of the inner support cylinder, the moment caused by $V_o a$ balances M_o or

$$(V_o)a + M_o = 0\,. \tag{D.3}$$

Equations D.1, D.2, and D.3 can be solved to obtain

$$M_o, N_o, V_o .$$

With these particular boundary conditions and with some geometries, the stress at ϕ_ℓ is higher than at ϕ_o. For such a case, the boundary loads at ϕ_ℓ can be found by equilibrium

$$V_o + V_\ell C\phi_\ell - N_\ell S\phi_\ell = 0$$
$$-N_o + V_\ell S\phi_\ell + N_\ell C\phi_\ell = 0$$
$$M_\ell + V_\ell y_\ell - N_o x_\ell - M_o = 0$$

or

$$\begin{aligned} M_\ell &= M_o + N_o x_\ell - V_o y_\ell \\ V_\ell &= N_o S\phi_o - V_o C\phi_\ell \\ N_\ell &= V_o S\phi_\ell + N_o C\phi_\ell \end{aligned} \quad . \tag{D.4}$$

Stresses are calculated, as outlined in Appendix C, using M_o, N_o or M_ℓ, N_ℓ, whichever yields higher stresses.

Appendix E

THERMAL ANALYSIS FOR ONE PLATE HOTTER THAN SURROUNDING PLATES

Appendix E. THERMAL ANALYSIS FOR ONE PLATE HOTTER THAN SURROUNDING PLATES

Plate stresses where one plate is hotter than the surrounding plates are analyzed as follows. The hot plate's boundaries are assumed to be restrained by the support cylinders and the other plates. Energy techniques can be applied. The scheme is to let $p = 0$, remove the inside support cylinder, and let the plate displace as a result of a temperature difference. Next, the inside plate boundary forces are applied to remove the thermal displacements which mathematically stated become

$$\frac{\partial U}{\partial M_o} = 0 = \int_0^{\phi_i} \frac{M}{EI}\frac{\partial M}{\partial M_o} a\phi d\phi \tag{E.1}$$

(reference Eq. A.4 for zero slope change at the origin),

$$\frac{\partial U}{\partial N_o} = \alpha \ell y \Delta T = \int_0^{\phi_i} \frac{M}{EI}\frac{\partial M}{\partial N_o} a\phi d\phi + \int_0^{\phi_i} \frac{\mathrm{N}}{\mathrm{AE}}\frac{\partial N}{\partial N_o} a\phi d\phi \tag{E.2}$$

(reference Eq. A.5, as N_o is adjusted to remove the thermal expansion in the direction of N_o), and

$$\frac{\partial U}{\partial V_o} = \alpha \ell_x \Delta T = \int_0^{\phi_i} \frac{M}{EI}\frac{\partial M}{\partial V_o} a\phi d\phi + \int_0^{\phi_i} \frac{\mathrm{N}}{\mathrm{AE}}\frac{\partial N}{\partial V_o} a\phi d\phi \tag{E.3}$$

(reference Eq. (A-6), as V_o is adjusted to remove the thermal expansion in the direction of V_o).

The solution of Eqs. E.1, E.2, and E.3 yield M_o, N_o, and V_o.

Appendix F

THERMAL STRESSES IN THE LONGITUDINAL DIRECTION OF THE PLATES

Appendix F: THERMAL STRESSES IN THE LONGITUDINAL DIRECTION OF THE PLATES

This analysis calculates the average stresses that occur in the longitudinal direction of the plates due to a difference in temperature between the support cylinders and the plates. Referencing the free body shown in Fig. F.1, equilibrium requires that

$$F_{ps} + F_o + F_i = 0 \ , \tag{F.1}$$

where

F_{ps} = the average force in the plates in the axial direction,
F_o = the average force in the outside support cylinder in the axial direction, and
F_i = the average force in the inside support cylinder in the axial direction.

Geometry requires

$$\delta_{ps} = \delta_o = \delta_i \ , \tag{F.2}$$

where

δ_{ps} = average axial displacement of the plates,
δ_o = average axial displacement of the outside support, and
δ_i = average axial displacement of the inside support.

Force-displacement relations for average or uniaxial conditions are

$$\begin{aligned} \delta_{ps} &= \frac{F_{ps}}{A_{ps}} \frac{\ell_{ps}}{E_{ps}} + \alpha_{ps} \ell_{ps} T_{ps} \\ \delta_o &= \frac{F_o}{A_o} \frac{\ell_o}{E_o} + \alpha_o \ell_o T_o \\ \delta_i &= \frac{F_i}{A_i} \frac{\ell_i}{E_i} + \alpha_i \ell_i T_i \ , \end{aligned} \tag{F.3}$$

where

ℓ = length of the element,
A = cross sectional area,
E = modulus of elasticity of element,
α = coefficient of thermal expansion of element, and
T = temperature of element.

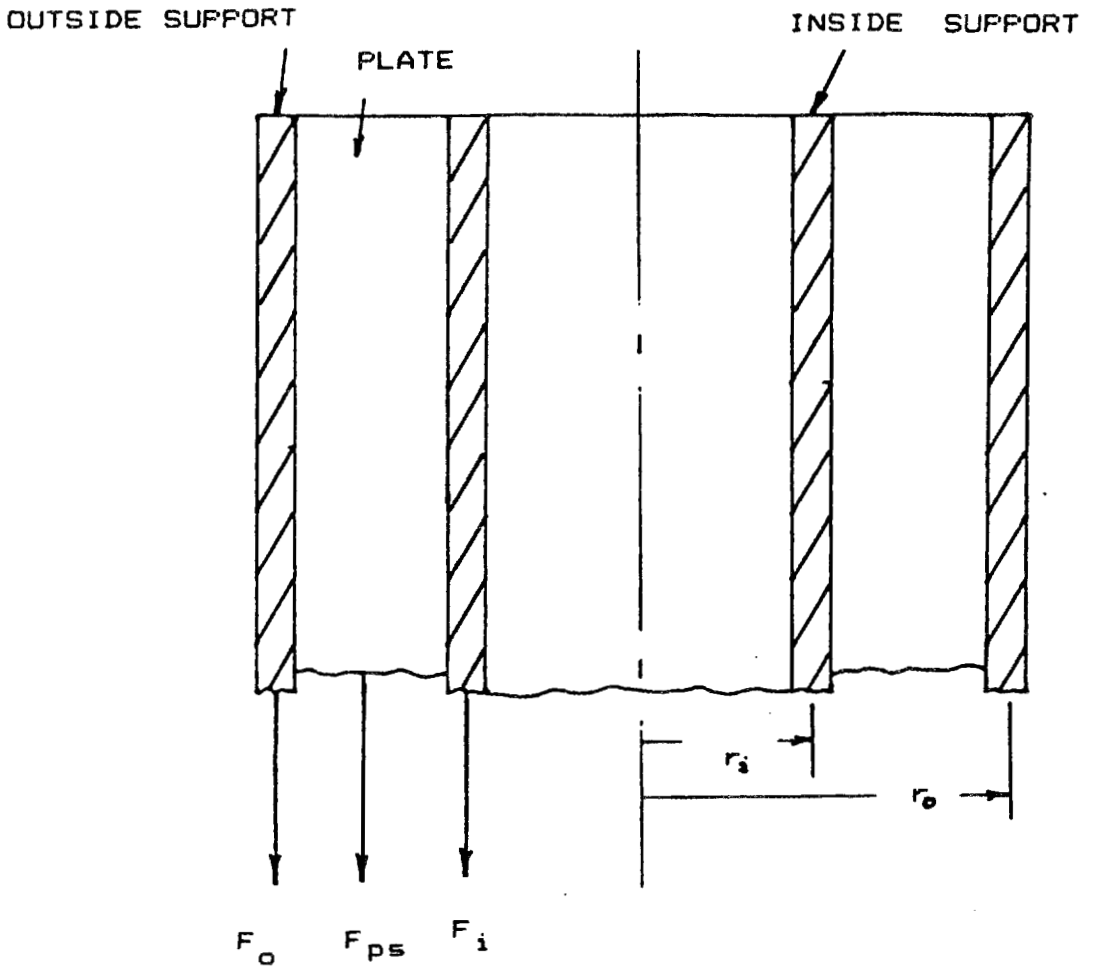

Fig. F.1. Free body of longitudinal thermal forces.

Assuming the same material properties, the solution is

$$F_{ps} = \frac{-E\alpha\left(A_o + A_i\right)}{\left(A_{ps} + A_o + A_i\right)}\Delta T A_{ps}$$

$$F_o = E\alpha\, A_o \Delta \mathrm{T}\left(1 - \frac{A_o + A_i}{A_{ps} + A_o + A_i}\right) \tag{F.4}$$

$$F_i = E\alpha\, A_i \Delta \mathrm{T}\left(1 - \frac{A_o + A_i}{A_{ps} + A_o + A_i}\right),$$

where ΔT is the average difference in temperature between the plates and supports.

The average stress is found using Eq. F.4 and dividing by the appropriate cross-sectional area.

Appendix G

THERMAL BUCKLING OF PLATES IN A LONGITUDINAL DIRECTION

Appendix G: THERMAL BUCKLING OF PLATES IN A LOGITUDINAL DIRECTION

In this development, it is assumed that the plate is at a constant temperature and that the side walls are at a different constant temperature. The effect of the involute curvature on the longitudinal buckling is assumed small; and the plate is approximated as a flat plate. It is anticipated that the buckling answer will be conservative as the transverse curvature will stiffen the plate against longitudinal buckling. In modeling the plate, the plate is allowed to expand more than the side walls longitudinally. It is assumed that a uniform compression stress field is applied to the plate and that a uniform tension field is applied to the side walls to produce enough deformation to equal the thermal expansion. In this model, the uniform plate stress field is applied by an axial load, where in reality the stress field is produced by side loads, Fig. G.1. Both types of loadings are statically equivalent. Referencing Fig. G.1, the plate boundary conditions are taken as:

$$w = 0; \quad \frac{\partial w}{\partial y} = 0 \qquad \text{at } y = 0 \text{ and } y = s, \tag{G.1}$$

and

$$w = 0; \quad \frac{\partial^2 w}{\partial x^2} + g\frac{\partial^2 w}{\partial y^2} = 0 \qquad \text{at } x = 0 \text{ and } x = \ell. \tag{G.2}$$

From plate theory, the governing equation is

$$\frac{\partial^4 w}{\partial x^4} + 2\frac{\partial^4 w}{\partial x^2 \partial y^2} + \frac{\partial^4 w}{\partial y^4} = -\frac{N_x}{D}\frac{\partial^2 w}{\partial x^2}, \tag{G.3}$$

where

$$D = \frac{Eh^3}{12(1-\gamma^2)}.$$

For a solution to Eq. G.3, assume a solution of

$$w = f(y) \quad S\frac{m\pi x}{\ell}, \tag{G.4}$$

which satisfies the boundary conditions of Eq. G.2 if m is restricted to an integer. Substituting Eq. G.4 into Eq. G.3 will yield a linear, fourth order differential equation. Note is made that because of the constraints on the boundaries, the buckling load will be higher than the load without constraints, therefore,

$$\frac{N_x}{D} > \frac{m^2\pi^2}{\ell^2}. \tag{G.5}$$

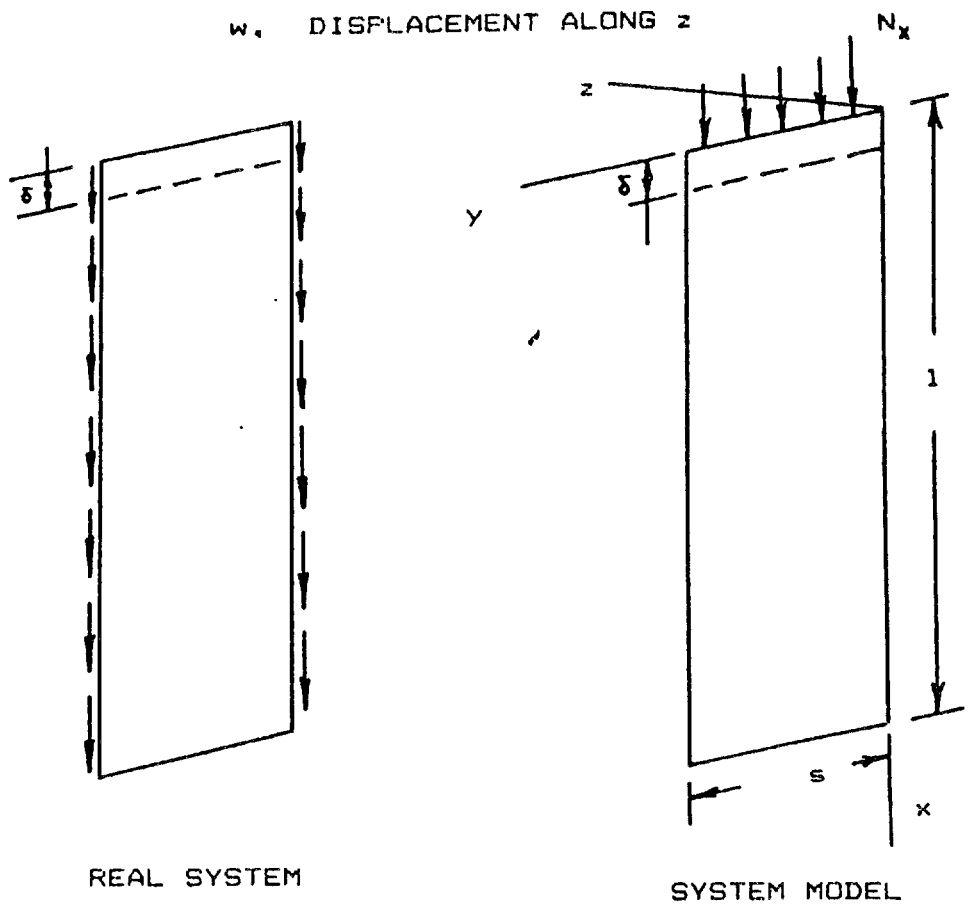

Fig. G.1. Thermal buckling load.

The solution takes the form

$$f(y) = C_1 e^{-Ay} + C_2 e^{Ay} + C_3 C(By) + C_4 S(By) , \tag{G.6}$$

where

$$A = \left[\frac{m^2 p^2}{\ell^2} + \sqrt{\frac{N_x}{D} \frac{m^2 p^2}{\ell^2}} \right]^{1/2}$$

and (G.7)

$$B = \left[\frac{-m^2 p^2}{\ell^2} + \sqrt{\frac{N_x}{D} \frac{m^2 p^2}{\ell^2}} \right]^{1/2} .$$

With the solution, Eqs. G.4 and G.6, the boundary conditions of Eqs. G.1 and G.2 can be reduced to

$$0 = \left[e^{-As} C(Bs) + (A/B)\, s(Bs) \right] C_1 + \left[e^{As} - C(Bs) - (A/B)\, s(Bs) \right] C_2$$

$$0 = \left[-Ae^{-As} + Bs(Bs) + AC(Bs) \right] C_1 + \left[Ae^{As} + Bs(Bs) - AC(Bs) \right] C_2 . \tag{G.8}$$

A solution to Eq. (G.8), other than the trivial solution, can be found by setting the determinant of the coefficients equal to zero or

$$0 = 2\,[1 - C(Bs) + Ch(As)] + [(-B/A) + (A/B)]\, s(Bs)\, sh(As) . \tag{G.9}$$

Note from Eq. G.7 that A and B are functions of N_x and m. The buckling load sought is the minimum value of N_x that satisfies Eq. G.9. The solution is found by assuming an integer, m, and solving for N_x. Starting with m equal to one, N_x can be found. Then, by systematically increasing m and solving for the corresponding N_x, eventually the minimum buckling load N_x can be found. The value of m that gives a minimum N_x is the number of half sine waves (buckles) predicted for the plate. The value of N_x times s (the arc length) times the number of plates equals F_{ps} of Appendix F. The buckling temperature can be found from the first of Eq. F.4.

Internal Distribution

1. C. W. Alexander
2. D. J. Alexander
3. R. R. Allen
4. E. E. Alston
5. J. L. Anderson
6. B. R. Appleton
7. R. L. Battise
8. R. E. Battle
9. R. S. Booth
10. R. A. Brown
11–15. J. H. Campbell
16. P. F. Cento
17. N. C. J. Chen
18. K. K. Chipley
19. J. A. Clinard
20. G. L. Copeland
21. J. M. Corum
22. J. R. Dixon
23. K. Farrel
24. D. K. Felde
25. M. L. Gildner
26. R. G. Gilliland
27. H. A. Glovier
28. R. C. Gwaltney
29. R. M. Harrington
30. J. B. Hayter
31. W. R. Hendrick
32. R. O. Hussung
33. D. T. Ingersoll
34–37. R. L. Johnson
38. J. E. Jones, Jr.
39. R. A. Lillie
40. M. A. Linn
41. A. T. Lucas
42. C. R. Luttrell
43. M. F. Marchbanks
44. J. A. March-Leuba
45. B. S. Maxon
46. G. T. Mays
47. S. V. McGrath
48. T. J. McManamy
49. G. R. McNutt
50. R. M. Moon
51. D. G. Morris
52. D. L. Moses
53. R. E. Pawel
54. H. R. Payne
55. F. J. Peretz
56. A. B. Poole
57. C. C. Queen
58. J. S. Rayside
59. J. B. Roberto
60. M. B. Ruggles
61. T. L. Ryan
62. D. L. Selby
63. H. B. Shapira
64. M. Siman-Tov
65. W. R. Swinson
66. R. P. Taleyarkhan
67. D. W. Thiesen
68. P. B. Thompson
69. K. R. Thoms
70. C. D. West
71. D. M. Williams
72. B. A. Worley
73. G. T. Yahr
74. G. L. Yoder
75. ORNL Patent Office
76–77. Central Research Library
78. Y-12 Technical Library, Document Reference
79–80. Laboratory Records
81. Labatory Records, RC

External Distribution

82. R. Awan, U.S. Department of Energy, NE-473, Washington, DC 20585
83. K. K. Conway, Laboratory Facilities Branch, U.S. Department of Energy, Oak Ridge Operations Office, CE-523, P.O. Box 2001, Oak Ridge, TN 37831-2001
84. R. R. Fullwood, Brookhaven National Laboratory, Upton, NY 11973
85. W. R. Gambill, Route 5, Box 220, Clinton, TN 37716
86. A. F. Henry, Professor, Department of Nuclear Engineering, Massachusetts, Institute of Technology, 77 Massachusetts Avenue, Cambridge, MA 02139
87. R. A. Hunter, Director, Office of Facilities, Fuel Cycel, and Test Programs, Nuclear Energy Division, U.S.Department of Energy, NE-47, Washington, DC 20585
88. T. L. Kerlin, University of Tennessee, College of Engineering, 315 Pasqua Engineering Building, Knoxville, TN 37996-2300
89. J. A. Lake, Manager, Nuclear Engineering and Reactor Design, Idaho National Engineering Laboratory, P.O. Box 1625, Idaho Falls, ID 83415
90. J. E. Mays, Research and Test Reactor Fuel Elements, Babcock and Wilcox Co., P.O. Box 785, Lynchburg, VA 24505
91. J. P. Mulkey, U.S. Department of Energy, NE-473, Washington, DC 20585
92. W. T. Oosterhuis, Materials Science Division, Office of Basic Energy Sciences, Office of Energy Research, U.S. Department of Energy, ER-132, Washington, DC 20585
93. J. M. Ryskamp, Idaho National Engineering Laboratory, P.O. Box 1625, Idaho Falls, ID 83415-3885
94. J. L. Snelgrove, Coordinator, Engineering Applications, RERTR Program, Argonne National Laboratory, 9700 South Cass Avenue, Argonne, IL 60439
95. I. Thomas, Director, Materials Science Division, Office of Energy Research, U.S. Department of Energy, ER-13, Washington, DC 20585
96. U.S. Department of Energy, ANS Project Office, Oak Ridge Operations Office, FEDC, MS-8218, P.O. Box 2009, Oak Ridge, TN 37831-8218
97. H. G. Wood, III, Associate Professor, Department of Mechanical and Aerospace Engineering, Thornton Hall, University of Virginia, Charlottesville, VA 22901
98. Office of Assistant Manager for Energy Research and Development, U.S. Department of Energy, Oak Ridge Operations Office, P.O. Box 2001, Oak ridge, TN 37831-2001

99–100. Office of Scientific and Technical Information, P.O. Box 62, Oak Ridge, TN 37831